
Unterschrift (Betreuer)



DIPLOMARBEIT

Design and Assembly of an Open Aperture Z-Scan Setup Based on a High-Power Femtosecond Oscillator

Ausgeführt am

Institut für Angewandte Physik &
Institut für Werkstoffwissenschaften und Werkstofftechnologie
der technischen Universität Wien

Unter der Anleitung von

ao.Univ.Prof. Dipl.-Ing. Dr.techn. Wolfgang Husinsky
und ao.Univ.Prof. Dipl.-Ing. Dr.mont. Jürgen Stampfl

durch

Wolfgang Steiger, BSc
0754329
Ruthgasse 21/22. 1190 Wien

Datum

Wolfgang Steiger, BSc

Abstract

The Z-Scan technique has become a standard method to characterize higher order nonlinearities such as two-photon absorption, which have found applications from 3D nanolithography to high-resolution 3D microscopy. However, usually Z-scan is performed at one single wavelength, providing only limited information on the spectral characteristic of compounds like photoinitiators and fluorescent dyes.

The aim of this thesis was to design a fully automated Z-Scan to characterize the nonlinear absorption properties of different compounds. This novel setup was based on a tunable high-power femtosecond oscillator, allowing scans from 690-1040 nanometers. A beam profiling method was implemented to efficiently extract the parameters of the focused beam. For the Z-Scan Rhodamine B was selected as reference material, since its cross section is well known in literature.

Compared to conventional amplified systems oscillator based Z-Scans can lead to thermal effects due to the high average power, which compromise the results. These effects were reduced by installing a beam chopper and adapting the software accordingly. The modifications allowed successful Z-Scan measurements which were comparable to Z-Scans using amplified systems.

Therefore, the oscillator based Z-Scan shows promise as a tool for spectral analysis of two-photon absorption.

Acknowledgments

First of all I would like to thank Jürgen Stampfl and Wolfgang Husinsky for the opportunity to write my thesis under their supervision. Their knowledge as well as the uncomplicated communication between the Institute of Materials Science and Technology (IMST) and the Institute of Applied Physics (IAP) allowed me to work in this fascinating field. I would also like to thank Aleksandr Ovsianikov for his constant support and knowledge of the laser system. His insights helped me to find the right solution for problems which otherwise would have taken weeks to figure out on my own. Also, thanks to Aliashgar Ajami. His expertise in the field of nonlinear absorption was crucial when modifying the setup.

I want to express my sincerest thanks to Peter Gruber who went far above and beyond the call of duty when working with me on the Z-Scan station. A year ago programming graphical interfaces and operating oscilloscopes via command lines seemed like an impossible task to me and I want to thank him for his patience and constant support.

Lastly, I want to thank the entire team of the Institute for Material Science and Technology who made working on this project a joy, irrespective of the duration or complexity of the experiments.

Contents

1	Introduction	1
2	Theory	3
2.1	Multi-Photon Absorption	3
2.2	Z-Scan	3
2.2.1	Setup	4
2.2.2	Phase Shift and Intensity	6
2.2.3	Transmittance	7
2.2.4	2PA Cross Section	9
2.3	Beam Expanders	10
2.3.1	Refractive Expanders	11
2.3.2	Reflective Expanders	11
2.4	Focused Gaussian Beam	12
2.4.1	Beam Waist	12
2.4.2	Beam Width	12
2.4.3	Intensity Profile of a Focused Gaussian Beam	13
2.4.4	Chromatic Aberation	14
2.4.5	Thermal Lensing	15
2.5	Image Analysis	15
2.5.1	Image Moments	16
3	Experimental Setup	17
3.1	MaiTai DeepSee	17
3.2	Waveplate and Beam-Splitter	18
3.2.1	Camera Profiler	19
3.2.2	uEye Camera and Mount	20
3.2.3	Image Fitting Optimization	21
3.2.4	Rayleigh Length and Focus	22
3.3	Reflective Beam Expander	23
3.4	Cuvette and Mount	24

3.5 Rhodamine B	24
4 Results and Discussion	27
4.1 Waveplate Calibration	27
4.2 Power Transmission	29
4.3 Beam Profiler	30
4.4 Z-Scan	34
4.4.1 Continuous Z-Scan	34
4.4.2 Lower Power Limit	37
4.4.3 Beam Chopper Mode	39
5 Conclusion	43
6 Supplements	45
Bibliography	67

Chapter 1

Introduction

The field of two-photon absorption (2PA) describes the third order nonlinear absorption process of femtosecond laser pulses [1]. It is used for multiphoton microscopy where the fluorescence induced by 2PA is measured [2]. The 2PA process is proportional to the squared intensity, therefore the fluorescence only takes place at the focal point. This allows intrinsic three dimensional resolution [3]. Due to deeper tissue penetration and less photodamage new imaging techniques are possible, which cannot be achieved using conventional confocal microscopy [4]. Aside from these applications, 2PA can also be used for nano lithography where high resolution scaffolds are created using two-photon polymerization (2PP) [5], which are required in biomedical applications [6, 7].

The focus of this group is on the fabrication of hydrogel scaffolds using custom water-soluble photoinitiators (PI) [8]. To measure the cross section of these PIs the Z-Scan technique was chosen, which is the most widespread method used to measure optical non-linearities of a material [9, 10]. For the scan a thin sample is moved in and out of the focus of a laser beam. The change in transmission is then used to calculate the 2PA coefficient [11].

The aim of this thesis was to automate the Z-Scan process. To achieve this, a software was written to control the laser, the automated stage, which moved the sample in and out of focus, the motorized wave plate, the oscilloscope and the USB-camera.

The Z-Scan setup was intended for the same laser, which was used for the 2PP process. Because of this we decided against an amplified system [12] to have similar parameters for the Z-Scan and the 2PP station. In the future this process can be easily adapted for tuneable scans of the nonlinear absorption spectrum without the need of readjusting the entire setup. This decision caused thermal effects due to the large repetition rate of the laser, which affected the measurements.

Chapter 2

Theory

2.1 Multi-Photon Absorption

In multiphoton absorption, the combined energy of two or more photons is used to bridge an energy gap, which would be too large for individual photons of the same wavelength. In theoretical terms this can be described as an excitation by a photon from a ground state into a short-lived virtual state with energy $h\nu_{\text{IR1}}$. The second photon's energy $h\nu_{\text{IR2}}$ can then excite the virtual state to an energy state above the gap. The second excitation needs to happen within the lifetime of the virtual state (see the Jablonski diagram in Fig. 2.1 A). If the photons have exactly the same energy $h\nu$ of approximately half the energy (twice the wavelength) of the gap the process is called degenerate (one-color) 2PA [13]. The idea was first postulated by Maria Goeppert-Mayer in 1931 [14]. Because of the technical limitations to create the necessary photon flux it took until 1961 to be proven by Kaiser and Garrett, who observed 2PA using a solid state laser [15].

The probability for 2PA absorption is given by the 2PA cross section in Goeppert-Mayer units defined as [16]

$$1 \text{ GM} = 10^{-50} \text{ cm}^4 \text{ s photon}^{-1} \text{ molecule}^{-1}. \quad (2.1)$$

The huge advantage of 2PA over 1PA is the fact that the absorption process only takes place in the focal plane of the laser as depicted Fig. 2.1 B and C) since the process is proportional to I^2 . This principle is used for 3D nanolithography [17] and for two- (or multi-)photon microscopy [18].

2.2 Z-Scan

The Z-Scan, introduced in 1990, has become a standard method for determining optical non-linearities [19, 20]. The technique has gained popularity due to its

relatively simple setup, which is shown in Fig. 2.2.

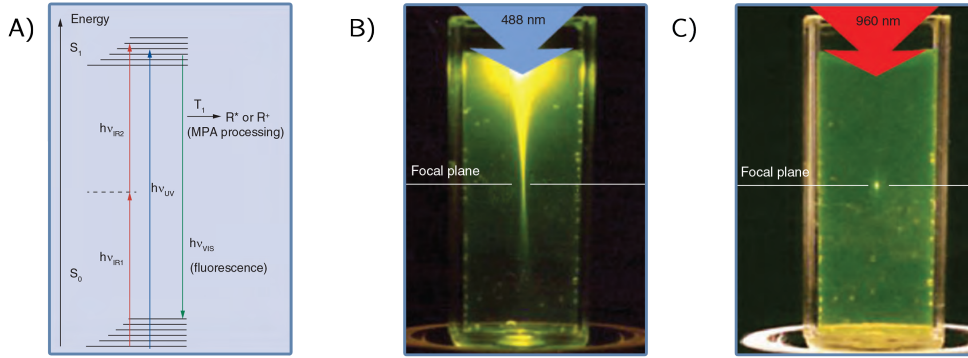


Fig. 2.1: 2PA theory: A) Jablonski diagram of the 2PA process. The first photon ($h\nu_{IR1}$) is absorbed into the virtual state. A second photon ($h\nu_{IR2}$) can then bridge the energy gap between E_0 and E_1 if it is absorbed within the lifetime of the virtual state. 2PA experiments: B) one photon absorption (1PA) of fluorescein at 488 nm and C) two photon absorption (2PA) at 960 nm. With 2PA the fluorescence is only observed at the focal plane. Image taken from [5]

2.2.1 Setup

A thin sample (sample length L smaller than the Rayleigh length λ_R) is moved in and out of a focused laser beam along an axis (usually called the z -axis, therefore the name of the technique). Ideally the laser focus is at the center of the stage. A photo diode at the end of the stage collects the transmitted light [11].

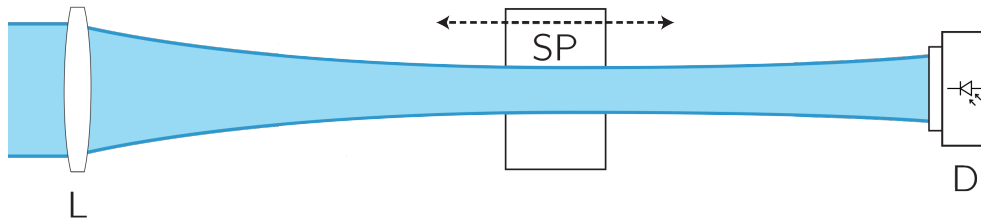


Fig. 2.2: A setup for an open aperture Z-Scan. Here, the thin sample (SP) is shifted in and out of lens's (L) focus. A photo diode (D) collects the transmitted light. The signals from the diodes are evaluated by an oscilloscope.

The discussed open aperture setup records drops in transmission, which can then be used to extract the 2PA behavior. It can be modified with an aperture in front of the diode to measure optical nonlinearities like refractive indices of materials (closed aperture Z-Scan). While the transmission curve $T(z)$ for the open aperture Z-Scan is a symmetric drop the closed aperture curve is a bit more complex (both transmission curves depicted in Fig. 2.3). Assuming a positive refractive nonlinearity, the sample acts as an additional lens depending on its position. In the far field the

transmission is relatively stable and the observed value is used for normalization. The closer the sample gets to the focus the more the positive refraction shifts the focus away from to the diode, therefore decreasing the transmitted light to the measurement diode. If the sample is moved past the focus (where the transmission curve has a zero-crossing), the positive refraction refocuses the beam which increases the transmission. The transmission returns to the normalized value in the far field [11].

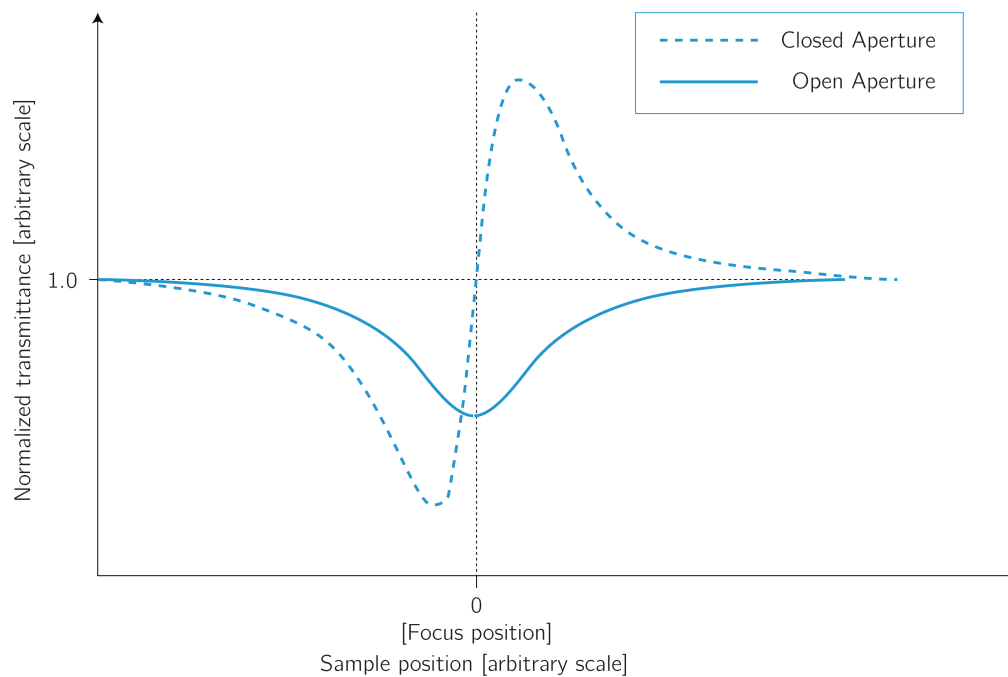


Fig. 2.3: Comparison between open aperture Z-Scan (solid line) for nonlinear absorption (NLA) and closed aperture Z-Scan (dotted line) for nonlinear refraction (NLR). The open aperture shows a symmetric drop in transmission around the focus. The curve for a negative NLR (sample acting as an additional lens with negative refraction) widens the beam before the focus (drop in signal) and focuses the beam after the focus position (increased signal), own representation based on [11].

2.2.2 Phase Shift and Intensity

To theoretically describe the Z-Scan, the effects of nonlinear self-action (nonlinear refraction (NLR) and nonlinear absorption (NLA)) need to be observed. Assuming nearly monochromatic laser light passing through the sample, the nonlinear self-action causes loss in transmission (ΔT).

The polarisation is given by [21]

$$\begin{aligned}
 P(t) = & \epsilon_0 \int_{-\infty}^{\infty} \chi^{(2)}(t-t_1)E(t_1)dt_1 + \int_{-\infty}^{\infty} \int_{-\infty}^{\infty} \chi^{(2)}(t-t_1, t-t_2)E(t_1)E(t_2)dt_1dt_2 + \\
 & + \int_{-\infty}^{\infty} \int_{-\infty}^{\infty} \int_{-\infty}^{\infty} \chi^{(3)}(t-t_1, t-t_2, t-t_3)E(t_1)E(t_2)E(t_3)dt_1dt_2dt_3 + \dots \quad (2.2)
 \end{aligned}$$

where $\chi^{(n)}$ describes the n-th order response or susceptibility function. The polarisation is dependent on the electric field

$$|E(t)| = \text{Re} \{ E(t) \cdot e^{i(kr-\omega t)} \}, \quad (2.3)$$

which varies slowly over time. For a single frequency input the field can be approximated in the external self-action limit [21]. For this to be applicable, the sample length L needs to be thin compared to the rayleigh length z_R . In addition, the intensities have to show an integrated phase shift of less than π . This allows us to write the polarisation as

$$P(t) = \epsilon_0 \chi E(t) = \epsilon \left[\chi^{(1)} + \chi^{(3)} \frac{|E(t)|^2}{2} \right] \cdot E(t). \quad (2.4)$$

The external self action limit later allows a separation of the wave equation into an equation describing the phase Φ and intensity I . For readability the time dependence was omitted in the following equations ($E = E(t)$, $P = P(t)$). The wave equation

$$\frac{d^2 E}{dz^2} - \frac{1}{c^2} \frac{d^2 E}{dt^2} = \mu_0 \frac{d^2 P}{dt^2} \quad (2.5)$$

is approximated by keeping only susceptibilities up to the 3rd order. Additionally the slowly varying envelope approximation (SVEA) [22] is used where the complex amplitude of the field $E(r, t)$ varies slowly with r and t . Thus, the higher ordered derivatives

$$\left| \frac{\partial^2 E}{\partial k^2} \right| \ll \left| k \cdot \frac{\partial E}{\partial k} \right| \quad \text{and} \quad \left| \frac{\partial^2 E}{\partial t^2} \right| \ll \left| \omega \cdot \frac{\partial E}{\partial t} \right| \quad (2.6)$$

are ignored. Applying these approximations leads to the wave equation

$$\frac{dE}{dz} + \frac{1}{c} \frac{dE}{dt} = i \frac{\omega}{2\epsilon_0 c} P. \quad (2.7)$$

A coordinate transformation applied to the system of the traveling wave ($\tau = t - \frac{z'}{x}$, $z' = z$) and with the substitution of the polarization (Eq. 2.4) gives

$$\frac{dE}{dz'} = i \frac{\omega}{2c} \cdot P = i \frac{\omega}{2c} \cdot \epsilon \left[\chi^{(1)} + \chi^{(3)} \frac{|E|^2}{2} \right] \cdot E. \quad (2.8)$$

Writing the electric field as $E = E_0 \cdot e^{i\phi}$ then allows splitting the equation into a real and an imaginary part:

$$\frac{dE_0}{dz'} = -\frac{\omega}{2c} \left[\text{Im} \{ \chi^{(1)} \} + \text{Im} \{ \chi^{(3)} \} \frac{E_0^2}{2} \right] \cdot E_0, \quad (2.9)$$

$$\frac{d\Phi}{dz'} = -\frac{\omega}{2c} \left[\text{Re} \{ \chi^{(1)} \} + \text{Re} \{ \chi^{(3)} \} \frac{E_0^2}{2} \right]. \quad (2.10)$$

Since $I \propto E_0^2$ it can be seen that $\chi^{(3)}$ causes phase shifts $d\Phi$ depending on the intensity. Rewriting Eqs. 2.9 and 2.10 in terms of intensity (considering only the nonlinear induced phase changes) leads to [21]

$$\frac{dI}{dz'} = -\underbrace{\frac{\omega}{2nc} \cdot \text{Im} \{ \chi^{(1)} \}}_{\alpha} \cdot I - \underbrace{\frac{\omega}{n^2 c^2 \epsilon_0} \cdot \text{Im} \{ \chi^{(3)} \}}_{\beta} \cdot I^2 \quad (2.11)$$

and

$$\frac{d\Phi}{dz'} = \frac{\omega}{c} \frac{1}{2n^2 c \epsilon_0} \text{Im} \{ \chi^{(3)} \} \cdot I, \quad (2.12)$$

with the linear refractive index n , the linear absorption coefficient α and the two photon absorption coefficient β .

2.2.3 Transmittance

The 3rd order nonlinearity is being observed which is now a complex quantity

$$\chi^{(3)} = \chi_R^{(3)} + \chi_I^{(3)} \quad (2.13)$$

and can be written as [19]

$$\chi_R^{(3)} = 2n_0^2 \epsilon_0 c \gamma, \quad \chi_I^{(3)} = \frac{n_0^2 \epsilon_0 c^2}{\omega} \cdot \beta \quad (2.14)$$

A Gaussian beam is used (TEM_{00}) to describe the electrical field's transmission [23]:

$$E(z, r, t) = E_0(t) \cdot \frac{\omega_0}{\omega(z)} \cdot \exp\left(-\frac{r^2}{w(z)} - \frac{ikr^2}{2R(z)}\right) e^{-i\Phi(z,t)}, \quad (2.15)$$

where $R(z)$ is the wavefront, $E_0(t)$ the amplitude of the electric field, $k = \frac{2\pi}{\lambda}$ the propagation vector and $e^{-i\Phi(z,t)}$ describes the radially symmetric phase shifts. The beam waist $\omega(z)$ along the z -axis is given by

$$\omega(z) = \omega_0 \sqrt{1 + \frac{z^2}{z_R^2}}. \quad (2.16)$$

with the Rayleigh length z_R , which will be discussed in detail in Chapter 2.4.3. Since changes in the refractive index Δn affect the phase shift the Eq. 2.12 is the following

$$\frac{d\Delta\Phi}{dz'} = \frac{\omega}{c} \Delta n I = \frac{2\pi}{\lambda} \cdot \Delta n I. \quad (2.17)$$

Changes in I (Eq. 2.11) are due to the linear (α) and nonlinear (β) absorption coefficients

$$\frac{dI}{dz'} = -\alpha I - \beta I^2. \quad (2.18)$$

It is important to note that while z denotes the position along the beam path z' describes the propagation depth. With the description of the Gaussian beam (Eq. 2.15) these two relations can be solved for the intensity (I_e) at the exit of the sample

$$I_e(z, r, t) = I(z, r, t) \cdot \frac{e^{-\alpha L}}{1 + q(z, r, t)} \quad (2.19)$$

and the phase shift

$$\Delta\Phi(z, r, t) = \frac{k\gamma}{\beta} \ln[1 + q(z, r, t)], \quad (2.20)$$

with $q(z, r, t) = \beta \cdot I(z, r, t) \cdot L_{eff}$. The effective sample length

$$L_{eff} = \frac{1 - e^{-2\alpha L}}{\alpha} \quad (2.21)$$

takes the linear absorption into account to express q describing the sample length without the effects of 1PA. Combining Eqs. 2.19 and 2.20 gives the complex field at the exit surface of the sample:

$$E_e = E(z, r, t) \cdot e^{-\frac{\alpha L}{2}} (1 + q(z, r, t))^{ik\gamma/\beta - \frac{1}{2}} \quad (2.22)$$

To describe the electric field E_a at the aperture (the aperture will later vanish for the open aperture Z-Scan) Huygens principle and a Hankel transformation of

zero order can be applied. An alternative approach used by Sheik-Bahae et al. [19] is the Gaussian decomposition, where the complex electric field after exiting the sample is decomposed into a summation of Gaussian beams. The individual beams are propagated towards the aperture, where they are resummed to E_a . The resulting expression contains both refractive and absorptive transmittances which are coupled by a factor $\frac{\beta}{2k\gamma}$. For open aperture Z-Scans the transmittance is insensitive towards beam distortions and therefore simplifies to a function depending solely on the nonlinear absorption.

The transmitted power $P(z, t)$ can therefore be obtained by integrating Eq. 2.22 over r without the inclusion of the free-space propagation process. This results in the transmitted power [11]

$$P(z, t) = P_i(t)e^{-\alpha L} \frac{\ln[1 + q(z, t)]}{q(z, t)} \quad (2.23)$$

with

$$q(z, t) = \beta \cdot I(t) \cdot L_{eff} \cdot \omega(z) \quad (2.24)$$

and

$$P_i = \frac{1}{2} \pi \omega_0^2 I_0(t). \quad (2.25)$$

Integrating Eq. 2.23 over time gives the normalized energy transmittance

$$T(z) = \frac{1}{\sqrt{\pi} q(z, 0)} \int_{-\infty}^{\infty} \ln(1 + q_0(z, 0) e^{-\tau^2}) d\tau. \quad (2.26)$$

For $|q(z, 0)| \leq 1$ this can be expressed as [24]

$$T(z) = \sum_{m=0}^{\infty} \frac{-q(z, 0)^m}{(m+1)^{\frac{3}{2}}}, \quad (2.27)$$

which is a more suitable form for numerical evaluation.

2.2.4 2PA Cross Section

The observed transmission $T(z)$ is used to extract the 2PA cross section σ_2 . By splitting the factor $q(z, 0)$ into a z -dependent ($\omega(z)^2$) and a constant (q_0) part, the factor $q(z, t)$ becomes [24]

$$q(z, 0) = q_0 \cdot \omega(z)^2 = \underbrace{\beta \cdot I_0 \cdot L_{eff}}_{q_0} \cdot \underbrace{\frac{1}{[1 + \frac{z^2}{z_R^2}]} }_{\omega(z)^2}. \quad (2.28)$$

The peak intensity (I_0) is required to extract σ_2 from q_0 . It is given by the beamwaist w_0 and peak power P_0 as

$$I_0 = \frac{2 \cdot P_0}{\pi w_0^2}. \quad (2.29)$$

The peak power cannot be measured directly for ultra short pulses. Therefore P_0 has to be calculated indirectly by taking the pulse energy E_p and pulse duration τ . Alternatively, the output power P_{out} and pulse repetition rate R can also express the pulse energy E_p . Including a geometrical factor, which accounts for the Gaussian profile [25], P_0 becomes

$$P_0 = 2 \cdot \sqrt{\frac{\ln(2)}{\pi}} \frac{E_p}{\tau} = 2 \cdot \sqrt{\frac{\ln(2)}{\pi}} \frac{P_{out}}{R \cdot \tau} \quad (2.30)$$

and I_0 (Eq. 2.29) turns to

$$I_0 = \frac{2 \cdot P_0}{\pi w_0^2} = 4 \cdot \sqrt{\frac{\ln(2)}{\pi}} \cdot \frac{P_{out}}{\pi w_0^2 R \cdot \tau}. \quad (2.31)$$

With 2.31 the factor q_0 can be written as

$$q_0 = \underbrace{\frac{\sigma_2 \lambda N_{A\rho}}{h \cdot c}}_{\beta} \cdot L_{eff} \cdot \underbrace{4 \cdot \sqrt{\frac{\ln(2)}{\pi}} \cdot \frac{P_{out}}{\pi w_0^2 R \cdot \tau}}_{I_0}. \quad (2.32)$$

The 2PA absorption coefficient β is obtained by [17]

$$\beta(\nu) = \frac{N}{E} \cdot \sigma_2 = \frac{N_{A\rho}}{h\nu} \cdot \sigma_2 = \frac{\lambda N_{A\rho}}{hc} \cdot \sigma_2 \quad (2.33)$$

with the two-photon cross section (σ_2) [GM], the Plank constant (h) [Js], the number density of molecules per volume (N) [m^{-3}] and the frequency of the laser light (ν) [Hz]. Rearranging Eq. 2.33 gives the 2PA cross section

$$\sigma_2 = \frac{h\nu\beta}{N_{A\rho}}. \quad (2.34)$$

2.3 Beam Expanders

In optics beam expanders are commonly used to enlarge a collimated beam. The centered laser beam enters into the expander, is expanded and then leaves again collimated. Generally speaking, there are two types of expanders: refractive expanders, which are based on lens effects, and reflective expanders, which use mirrors to widen the beam size. Since the refractive designs are based on lens effects they are susceptible to chromatic aberration (as discussed in Chapter 2.4.4).

2.3.1 Refractive Expanders

The two most used designs based on a system of lenses are the Galilean and Keplerian expanders [26]. A Galilean beam expander usually consists of a negative and a positive lens, which is visualized in Fig. 2.4 A. The Keplerian beam expander is comprised of two lenses with positive focal length.

Keplerian expanders are easy to build and are used in interferometric systems because the focal spot allows spatial filtering (for example placing a pinhole at the focal point). This focal spot can cause air between the lasers to heat up at high laser powers, deflecting light rays and potentially leading to wavefront errors. As a result, beam expanders in high powered laser optics are Galilean. Due to the missing focal point between the lenses, the Galilean design allows working at higher powers and has a more compact design.

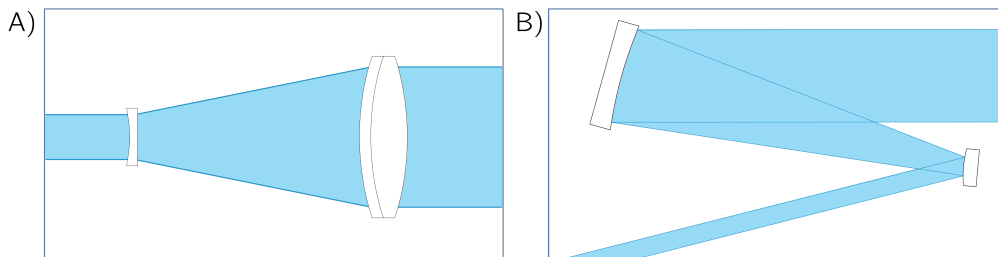


Fig. 2.4: A) Beam path of a Galilean beam expander consisting of a negative objective lens and a positive image lens. Own representation based on [26]. B) A convex mirror expands the beam upon a larger concave mirror, which again collimates the beam, own representation based on Thorlabs data sheet [27]

2.3.2 Reflective Expanders

A reflective beam expander consists of two mirrors as depicted in Fig. 2.4 B. The convex front mirror expands the beam, reflecting it onto a larger concave mirror to collimate the beam [26]. For this reason, there is no focal shift due to chromatic aberration compared to refractive expanders.

Due to the geometry of this construction the exit angle is different from the entrance angle. This means that contrary to the refractive expander the beam path has to be realigned for this component whereas a Galilean expander can simply be placed into the path.

2.4 Focused Gaussian Beam

2.4.1 Beam Waist

When focusing a laser with a lens the waist at the focal plane ω_0 is given by the geometries of the lens [28]

$$2 \cdot \omega_0 = \frac{4 \cdot \lambda \cdot f}{\pi \cdot D}, \quad (2.35)$$

where λ is the laser's wavelength, f the focal length of the lens and D the diameter of the lens. This equation assumes that the beam is of the same size as the lens diameter D . For smaller beams the diameter of the incoming collimated beam has to be used. Therefore, a larger beam leads to a smaller beam waist ω_0 and a higher intensity density. This relation is the reason for the use of beam expanders in the Z-Scan setup. The expander enlarges the beam in order to gain higher energy density at the focal point.

2.4.2 Beam Width

The width of the beam $\omega(z)$ for any position along the z -axis can be described by the following relation [29]

$$\omega(z) = \omega_0 \cdot \sqrt{1 + \left(\frac{z}{z_R}\right)^2}, \quad (2.36)$$

where z is the distance along the z -axis, ω_0 the beam waist and z_R the Rayleigh length which is defined by [30]

$$z_R = \frac{\pi \cdot \omega_0^2}{\lambda}. \quad (2.37)$$

It is the distance z_R from the center, where the area of the beam has doubled (or alternatively $\omega(z_R) = \sqrt{2}\omega_0$ as shown in Fig. 2.5). With z_R and ω_0 the beam can be fully characterized. For larger distances from the focus $\omega(z)$ increases linearly, which gives the total divergence angle

$$\Theta = 2 \cdot \theta \approx 2 \cdot \frac{\lambda}{\pi \omega_0}. \quad (2.38)$$

As this angle is inversely proportional to ω_0 a smaller beam shows a larger divergence behavior. Because of this relation, beam expanders are also used in optical setups where the laser beam needs to travel longer distances. In these systems a beam expander increases the beam size in order to reduce the beam divergence angle. That way, a better collimation is upheld for longer optical paths.

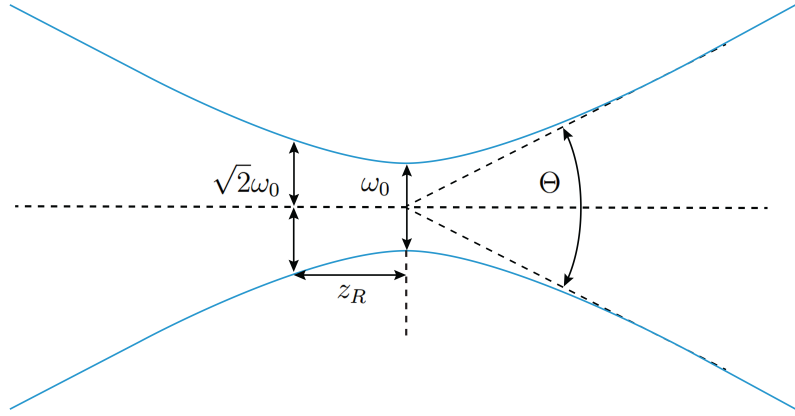


Fig. 2.5: Width $w(z)$ of a Gaussian beam along the z -axis. The Rayleigh length z_R is defined as the distance from the waist ω_0 where the width has increased to $\sqrt{2} \cdot \omega_0$. Θ is the total divergence angle.

2.4.3 Intensity Profile of a Focused Gaussian Beam

The previously discussed beam waist ω_0 can be described using a 2d-Gaussian distribution

$$I(\tilde{x}, \tilde{y}) = I_0 \cdot e^{-\frac{1}{2} \cdot \left(\frac{\tilde{x}-x_0}{\sigma_x}\right)^2} \cdot e^{-\frac{1}{2} \cdot \left(\frac{\tilde{y}-y_0}{\sigma_y}\right)^2}, \quad (2.39)$$

which describes the local intensity distribution of the beam at any position z along the axis. The waist is then defined as the radial distance where the intensity drops to $I_0 \cdot e^{-2}$. This can easily be extracted from Eq. 2.39 which was simplified to

$$I(x, y) = I_0 \cdot e^{-\frac{1}{2} \cdot \left(\frac{x}{\sigma_x}\right)^2} \cdot e^{-\frac{1}{2} \cdot \left(\frac{y}{\sigma_y}\right)^2} \quad (2.40)$$

by the use of coordinate translation ($x = \tilde{x} - x_0$, $y = \tilde{y} - y_0$). To extract the radial position r_x of the waist the requirement is

$$I(r_x, y) = I_0 \cdot e^{-2} \cdot e^{-\frac{1}{2} \cdot \left(\frac{y}{\sigma_y}\right)^2} = I_0 \cdot e^{-\frac{1}{2} \cdot \left(\frac{r_x}{\sigma_x}\right)^2} \cdot e^{-\frac{1}{2} \cdot \left(\frac{y}{\sigma_y}\right)^2}. \quad (2.41)$$

After canceling, this simplifies to

$$e^{-2} = e^{-\frac{1}{2} \cdot \left(\frac{r_x}{\sigma_x}\right)^2}, \quad (2.42)$$

$$2 = \frac{1}{2} \cdot \left(\frac{r_x}{\sigma_x}\right)^2. \quad (2.43)$$

From this derives the relation between σ_x and r_x

$$r_x = 2 \cdot \sigma_x. \quad (2.44)$$

The same approach can be used for r_y :

$$r_{x,y} = 2 \cdot \sigma_{x,y}. \quad (2.45)$$

An alternative description for the beam shape is the full width at half maximum (FWHM), where the characteristic point is the distance from the distribution's peak to the point where the intensity has dropped to $\frac{I_0}{2}$:

$$I(x_f, y) = \frac{1}{2} \cdot I_0 \cdot e^{-\frac{1}{2}(\frac{y}{\sigma_y})^2}, \quad (2.46)$$

$$I(x_f, y) = I_0 \cdot \frac{1}{2} \cdot e^{-\frac{1}{2}(\frac{y}{\sigma_y})^2} = I_0 \cdot e^{-\frac{1}{2}(\frac{x_f}{\sigma_x})^2} \cdot e^{-\frac{1}{2}(\frac{y}{\sigma_y})^2}, \quad (2.47)$$

$$\ln(\exp(-\frac{1}{2} \frac{x_f^2}{\sigma_x^2})) = \ln(\frac{1}{2}) = \ln(2^{-1}) = -\ln(2), \quad (2.48)$$

$$x_f = \sqrt{2 \cdot \ln(2)} \cdot \sigma_x. \quad (2.49)$$

This is also valid for y_f . A radially symmetric Gaussian distribution is assumed ($r_x = r_y = \omega_0$ and $x_f = y_f = d_f$) for a perfect Gaussian laser beam.

2.4.4 Chromatic Aberation

When working with optical lenses there are a variety of optical aberrations (astigmatism, chromatic aberration, coma, defocus, distortion, spherical aberration, tilt) [31]. Since the refractive index is dependent on the wavelength, the focus of a lens is different for varying wavelengths (see Fig. 2.6 A). This phenomenon is called chromatic aberration and played an important part in designing the Z-Scan setup. This aberration can be reduced by achromatic lenses (Fig. 2.6 B), own representation based on [31]), which consist of a system of two lenses (one convex, the other concave) made from two different types of optical glass and therefore have different refractive indices.

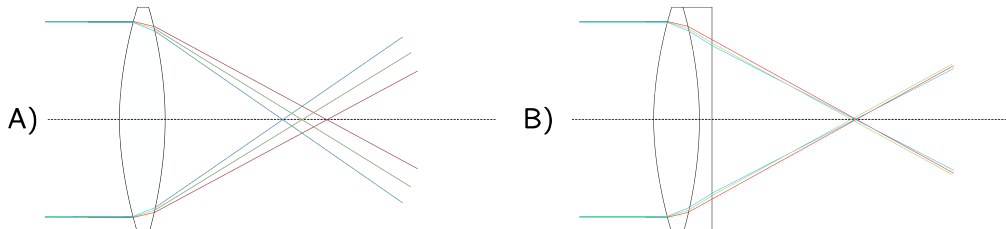


Fig. 2.6: A) chromatic aberration of a biconvex lens, B) achromatic doublet to reduce the aberration. Own representation based on [31]

2.4.5 Thermal Lensing

When exposing a sample to a high-powered laser signal, the sample is heated up over time. This can cause thermal effects which affect the measured data [32, 33]. The absorbed light heats up the sample and the resulting temperature gradient causes a variation in the sample density. This in turn changes the refractive index and leads to a lens-like behavior of the sample [34] (as illustrated in Fig. 2.7). The heating persists over a characteristic thermal time [35]

$$t_c = \frac{w_0^2}{4D}, \quad (2.50)$$

after which the sample has returned to thermal equilibrium. This coefficient depends on the beam waist w_0 and the thermal diffusion coefficient D [$\frac{\text{cm}^2}{\text{s}}$] of the observed material. With D typically in the range of 10^{-3} to $6 \cdot 10^{-3} \frac{\text{cm}^2}{\text{s}}$ for liquids, the condition for the characteristic time is met for lasers with a repetition rate higher than 0.1 KHz [32]. For high-repetition lasers the sample does not return to the equilibrium temperature between the pulses and therefore the transmission signal is no longer affected by just the 2PA behavior. Since the repetition rate of the MaiTai laser used in the experiments is in dimensions of MHz, the thermal effects were indeed affecting the measurements since the sample did not return to the equilibrium state. To allow return to thermal equilibrium, a beam chopper can be used which exposes the sample for about 2 ms with an off time of 48 ms [36].

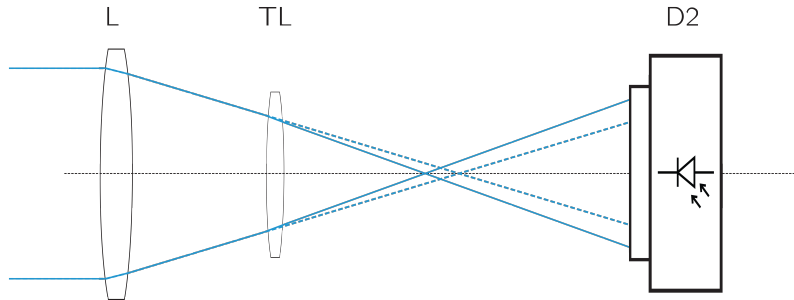


Fig. 2.7: Visualization of the thermal lens. If the characteristic time t_c is too long for the system to return to thermal equilibrium the shifts in density due to the heating cause the sample to act as an additional lens (TL) in the optical system.

2.5 Image Analysis

A secondary goal of this thesis was to write a program, which automatically analyzed a recorded laser beam (see Chapter 6). This can be done by fitting a 2D Gaussian distribution using the mathematical method of image moments.

2.5.1 Image Moments

In image analysis image moments are used to describe a given picture. Depending on the order of the moment the average or variance of a distribution can be extracted.

Given a continuous 2D distribution $f(x, y)$, the raw moment of order $p + q$ is defined as [37]

$$M_{pq} = \int_{-\infty}^{+\infty} \int_{-\infty}^{+\infty} x^p y^q f(x, y) dx dy \quad (2.51)$$

with the central moments given by

$$\mu_{pq} = \int_{-\infty}^{+\infty} \int_{-\infty}^{+\infty} (x - \bar{x})^p (y - \bar{y})^q f(x, y) dx dy \quad (2.52)$$

For a discrete distribution (i.e. a pixel image) the equations 2.51 and 2.52 are modified to [37, 38]

$$M_{ij} = \sum_x \sum_y x^i y^j I(x, y) , \quad (2.53)$$

$$\mu_{pq} = \sum_x \sum_y (x - \bar{x})^p (y - \bar{y})^q f(x, y) dx dy \quad (2.54)$$

With the mean values

$$\bar{x} = \frac{M_{10}}{M_{00}} , \quad \bar{y} = \frac{M_{01}}{M_{00}} . \quad (2.55)$$

These mean values offer estimates for the position of the peak intensity of a Gaussian distribution. The second order moments (M_{20}, M_{02}) correspond to the variances of the distribution (μ_x, μ_y).

Chapter 3

Experimental Setup

The Z-Scan station is powered by a femtosecond pulsed laser (Spectra Physics, MaiTai DeepSee). The beam is directed through a number of optical components (see Fig. 3.1) onto a lens which then focuses the beam onto a sample. The sample is placed upon a motorized stage (SMAC, LCS16-025-2(4)5) with an operating distance of 0-25.8 millimeters. The stage is accessed by a one-axis controller (SMAC, LCC-10). While the stage is moving the sample in and out of focus, a measurement diode is recording the transmitted light. Simultaneously, a reference diode provides a signal to compensate systematic signal fluctuations. The signals of both diodes are measured using an oscilloscope (Rigol, DS4024).

3.1 MaiTai DeepSee

The MaiTai DeepSee is a titanium-doped sapphire (Ti-sapphire) tunable laser, which emits light in the range of 690-1040 nm. Ti-sapphire lasers are pumped using a second laser in the green spectral range (around 520 nm). The sapphire's large thermal conductivity reduces the thermal effects, while the doped titanium has a large gain bandwidth, allowing the laser to generate pulses in the fs range.

The pulses are achieved by mode locking where a fixed phase between the longitudinal waves within the laser's cavity causes interference. The light is not emitted as a constant wave (cw), but as a train of pulses. To achieve the ultra short pulses the MaiTai uses passive mode locking based on the Kerr lens effect [39]. The Kerr lens describes the change in the material's refractive index depending on the beam's intensity. Therefore, the material acts as a lens for high intensities. The MaiTai also uses regenerative mode locking [40] to uphold the laser's stability [41].

The MaiTai's maximum laser power is 2.34 W (see Chapter 4.1). The wavelength tuning is achieved by dispersive elements (prisms) and selective filtering using adjustable slits. The laser is operated at a constant temperature of 21 °C using an

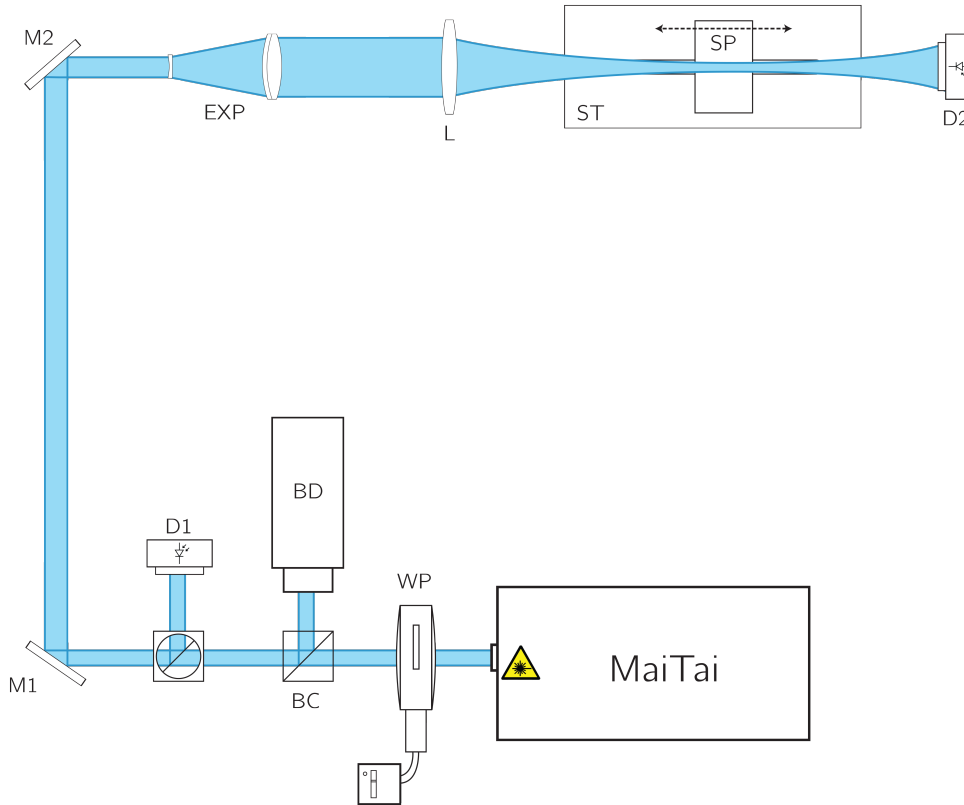


Fig. 3.1: Beam path from the MaiTai-laser. Components: waveplate (WP), beam splitter cube (BC), beam dump (BD), beam sampler (BS), two mirrors (M1, M2), reference diode (D1), measurement diode (D2), beam expander (EXP), lens (L) and sample (SP) placed onto a moveable stage (ST).

external chiller. Further data for the laser can be found in Tab. 3.1.

3.2 Waveplate and Beam-Splitter

Waveplates are optical devices, which change the laser beam's polarisation. They are constructed of birefringent material, which shows different refractive indices depending on the polarization. Waveplates are also known as retarders, since one polarization direction is retarded while progressing through the material. This in turn changes the relative phase between two components of polarization [42].

A motorized rotation stage (Thorlabs, PRM1Z8) controls the angle of the setup's waveplate in order to regulate the beam polarisation after emission from the laser. Afterward, the light is directed through a beam splitter cube. The cube uses total reflection to allow only a fraction of the polarized light to pass through. The rest is directed into a beam dump by means of total internal reflection. This allows the regulate the laser power from up to 2.2 W down to 36 mW (data for 800 nm). The beam power P_{out} after the beam splitter is given by [43]

MaiTai DeepSee data	
Pulse width (τ)	100 fs
Tuning range (λ)	690-1040 nm
Repetition rate (R)	80 MHz
Average power	2.1 W
Beam diameter ($\frac{1}{e^2}$)	< 1.2 mm
Beam divergence	< 1.2 mrad
Operating temperature	20 – 25 °C

Tab. 3.1: MaiTai DeepSee data taken from the data sheet [41]

$$P_{out} = A_0 + A \cdot \sin(b \cdot \theta + \phi)^2 \quad (3.1)$$

and depends on the waveplate's angle (θ), the initial offset (A_0), the amplitude (A), the phase (ϕ) and the periodicity (b). A_0 results from the fact that the waveplate is never filtering 100 % of the beam's energy, so there is always a minimal, non-zero power value.

3.2.1 Camera Profiler

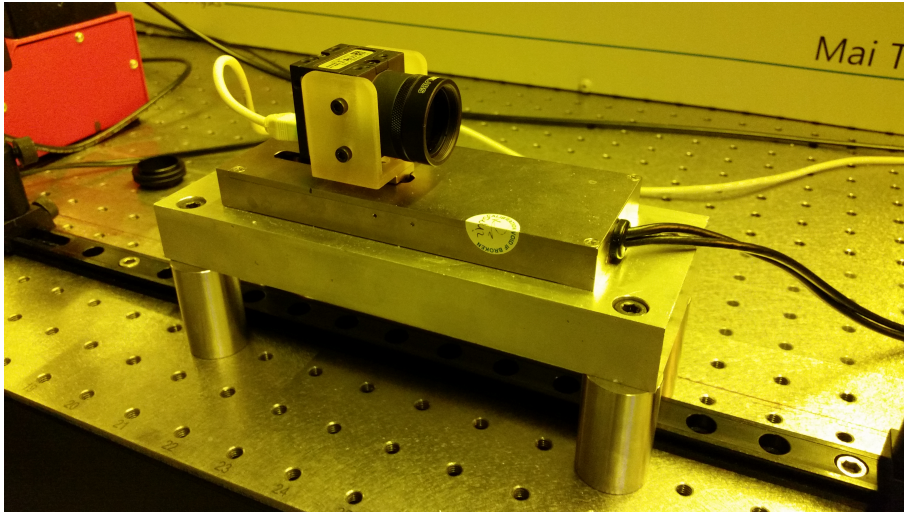


Fig. 3.2: Mounted uEye camera on the motorized stage with neutral density (ND) filters to reduce the intensity on the camera's chip.

Because of the MaiTai's wavelength range in the visible to near infrared spectrum (690 nm - 1040 nm) a USB operated camera was used for the profiling. An alternative approach to measure the beam profile is the Knife Edge method [44] where a sharp and thin object is moved between the beam and the measuring diode, gradually

decreasing the transmitted intensity. This results in an error function (Eq. 3.2) from which the beam shape can be extracted.

The camera approach was preferred over the Knife Edge method as it allowed live imaging without the need for an additional automated component like a moveable razor knife. In addition, the high resolution of the camera's chip was more than sufficient to directly extract the correct beam shape from the image.

3.2.2 uEye Camera and Mount

The uEye camera (IDS Imaging Development Systems, UI-1580SE-C-HQ) is a USB operated camera based on a CMOS (complementary metal-oxide-semiconductor) image sensor. The camera has a resolution of 2560×1920 with a $2.2 \mu\text{m}$ per pixel. The quantum efficiency (percentage of photons hitting the device's chip which produce carrier charges) of the camera can be seen in Fig. 3.3. At higher wavelengths (close to 1000 nm) the camera's sensitivity is clearly lower, which makes profiling at the higher wavelengths a more time-consuming task compared to the visible spectral range.

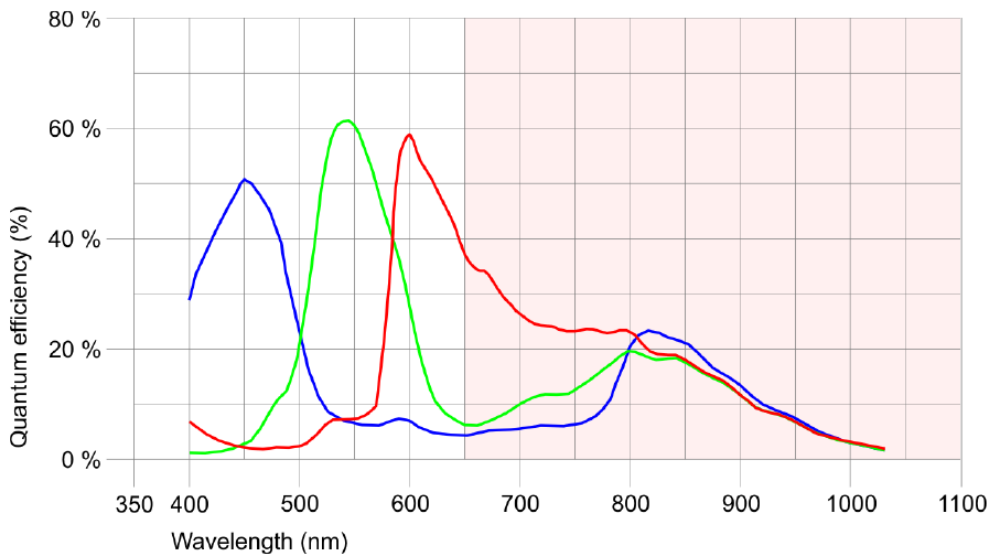


Fig. 3.3: Quantum efficiency (percentage of photons arriving at the chip which produce charge carriers) for the uEye camera. The quantum yield decreases significantly for the IR-spectrum where more measurements were required to reduce the measurement error and extract reliable data. Image taken from [45]

It was important that the center of the camera was placed at the same position as the center of the cuvette. This allowed a user-friendly alignment of the sample along the entire stage using the live image of the camera.

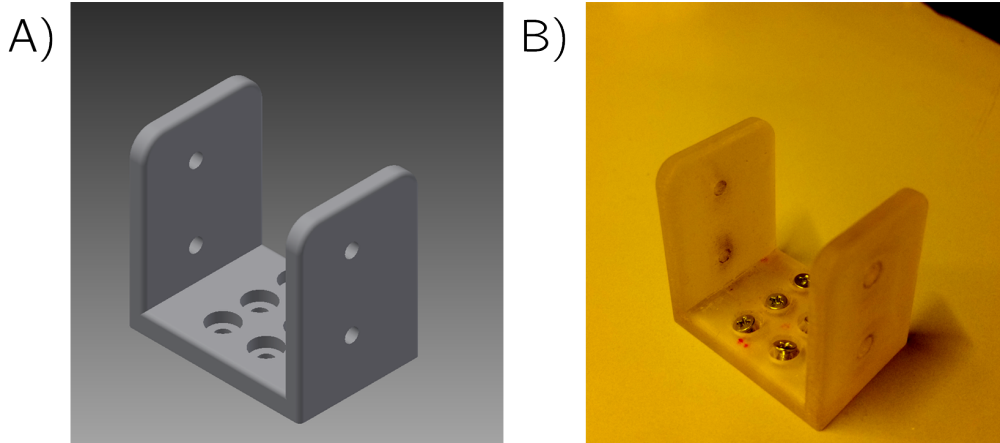


Fig. 3.4: Mount for the uEye camera to place the center of the camera where the window of the cuvette would be: A) CAD model, B) printed mount.

3.2.3 Image Fitting Optimization

An algorithm was developed to extract the characteristic data from the 2d Gaussian beam. The image moments method (discussed in Chapter 2.5) returned an initial estimate of the center and widths of the distribution. Since in numerical analysis the rounding error is lower for numerical integration compared to differentiation the error function was used for this calculation. This was done since the error function

$$\operatorname{erf}(x) = \frac{2}{\sqrt{\pi}} \int_0^x e^{-u^2} du \quad (3.2)$$

is the integral of the Gaussian function and therefore depends on the same parameters (similar to the knife edge method). Optimizing with the least square method [46] returns the distribution parameters. While this approach yielded results it was not a time efficient solution: As the image moments summed over the discrete grid (2560×1920 pixels) of the camera, the computation duration for one image took up to 7 seconds. This time had to be reduced to a fraction of a second for the profiler to work in an appropriate amount of time.

In order to achieve this the algorithm was modified to scan the entire image to find the pixel with the highest intensity (0 black, 255 white), which served as an estimate of the center of the beam. This pixel was then used as the center of a square which was cut out from the original pixel to have less data points for computing (visualized in Fig. 3.5).

Assuming a beam waist of $25 \mu\text{m}$ and a pixel resolution of $2.2 \mu\text{m}$ an array of 250×250 pixels contained all the necessary data for the fit, reducing the amount of data points by 78%.

From this reduced data the characteristic quantities of the Gaussian distribution (height (I_0), relative center positions (x_{rel} , y_{rel}), widths (w_x , w_y)) were extracted

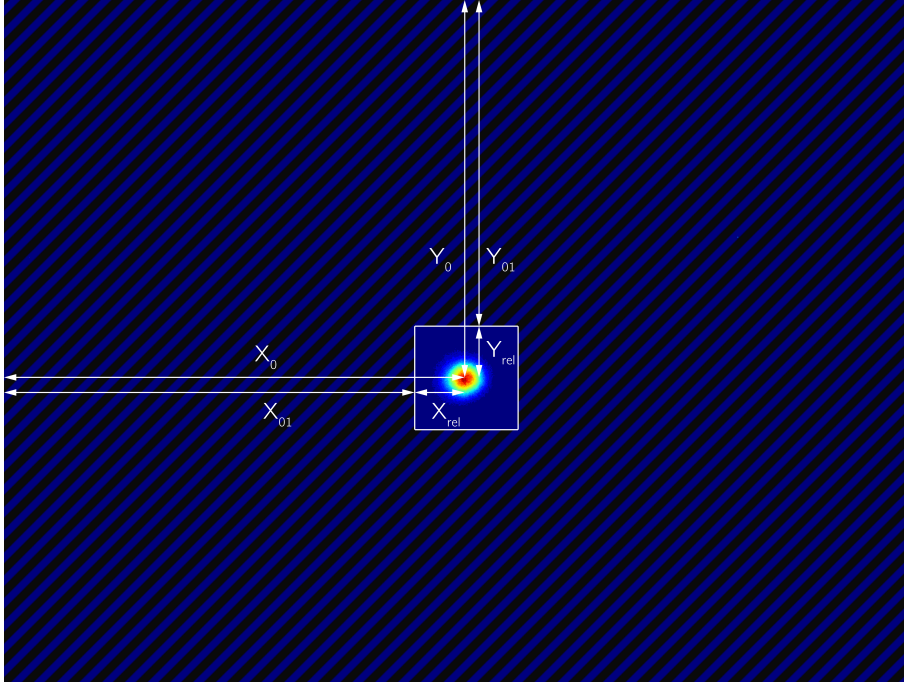


Fig. 3.5: Visualization of the image reduction algorithm. The striped area represents the data ignored for the image moments algorithm to increase the program's speed. The position of the cut out image (x_{01}, y_{01}) was saved so that the center position of the Gaussian (x_0, y_0) distribution could be calculated from the relative center positions x_{rel}, y_{rel} .

with the least square method. The center positions relative to the reduced 250×250 image were then extrapolated to the original image size. This was achieved by the program saving the x- and y-positions where the image had been cut out (x_{01}, y_{01}) so that the absolute center positions (x_0, y_0) , could be calculated by

$$x_0 = x_{rel} + x_{01}, \quad y_0 = y_{rel} + y_{01}. \quad (3.3)$$

3.2.4 Rayleigh Length and Focus

The process of extracting the characteristic data from the Gaussian beam $(I_0, x_0, y_0, w_x, w_y)$ was repeated for multiple stage positions. The obtained results allowed fitting the beam waist $\omega(z)$ (Eq. 2.36), extracting the Rayleigh length z_R and determining the focal position z_0 along the stage by shifting the symmetry of the beam waist

$$\omega(z) = \omega_0 \cdot \sqrt{1 + \left(\frac{z - z_0}{z_R}\right)^2}. \quad (3.4)$$

3.3 Reflective Beam Expander

The initial Z-Scan setup (Fig. 3.1) contained a refractive beam expander (Chapter 2.3) to expand the collimated beam onto the focal lens. However due to chromatic aberration (measurements can be found in Tab. 4.2) the shift in focus was too large for the stage, which would have required modified setup for each wavelength. The refractive expander was therefore replaced with a 4 x reflective expander. Due to the alternate beampath the Z-Scan station had to be rearranged as displayed in Fig. 3.6.

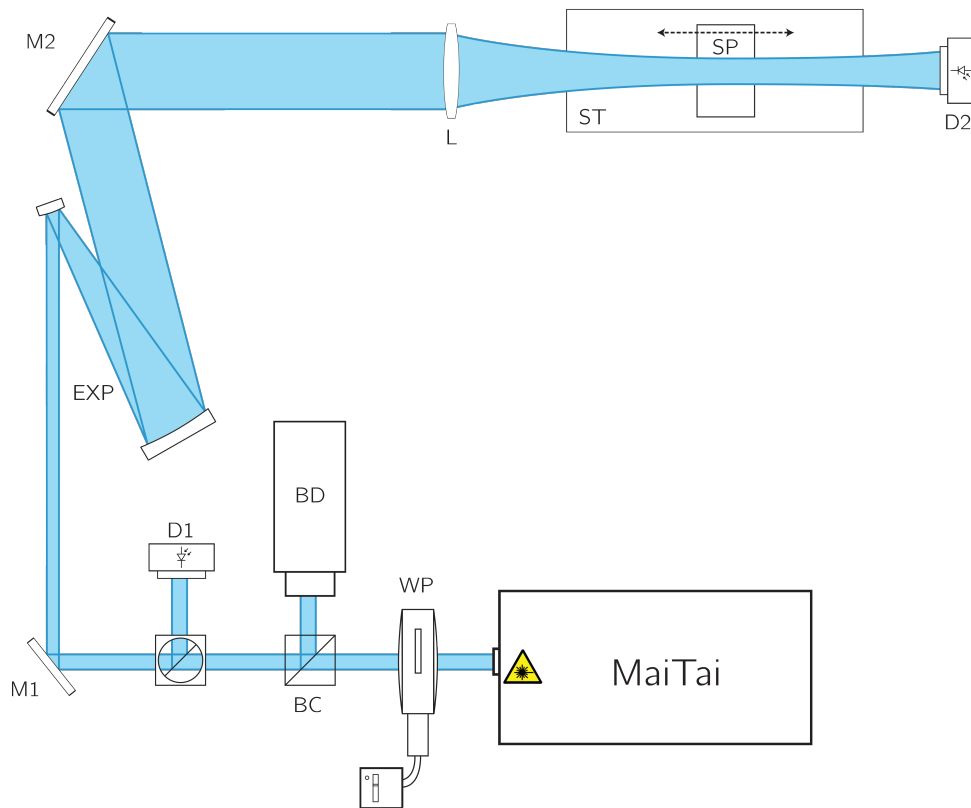


Fig. 3.6: Rearranged beam path after the refractive beam expander had been replaced by a reflective one. Components: waveplate (WP), beam splitter cube (BC), beam dump (BD), beam sampler (BS), two mirrors (M1, M2), reference diode (D1), measurement diode (D2), beam expander (EXP), lens (L) and sample (SP) placed onto a moveable stage (ST).

3.4 Cuvette and Mount

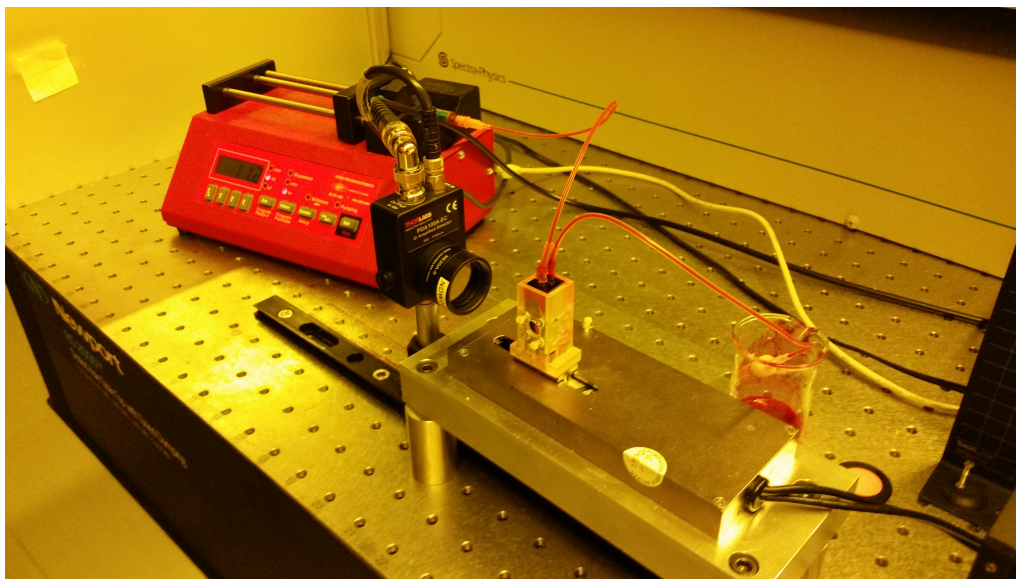


Fig. 3.7: Moveable stage with mount and cuvette on top.

The measurement diode at the end of the stage collects the transmitted data, while the pump is regulating the material flow through the cuvette.

A cuvette was used to hold the liquid material during the experiment. For the Z-Scan experiment a quartz cuvette was chosen since quartz shows high transmission behavior at the wavelengths of the MaiTai [47].

Initially, a cuvette with a sample length L of 1 mm and a cuvette window of 1 mm was used. For later experiments it was replaced by a cuvette with 0.2 mm sample length and a window of 6.5 mm.

A mount was designed to place the cuvette onto the moveable stage. It was modeled to keep the cuvette stable, as to not distort the measurements. Moreover, an additional lateral opening enabling future fluorescence observations. As the initial sample holder design still allowed small vibrations of the cuvette, a second holder was devised, which allowed to fixate the cuvette via plastic bolts (Fig. 3.8 A). For later experiments a mount was constructed which held the cuvette (Fig. 3.8 B) in place by means of elastics placed around two bolts. This was done in order to avoid damaging the cuvette when screwing the plastic bolts too tightly.

3.5 Rhodamine B

As the intention of this project was to build an automated Z-Scan station, Rhodamine B was chosen as a reference material for the quality of the Z-Scan results.

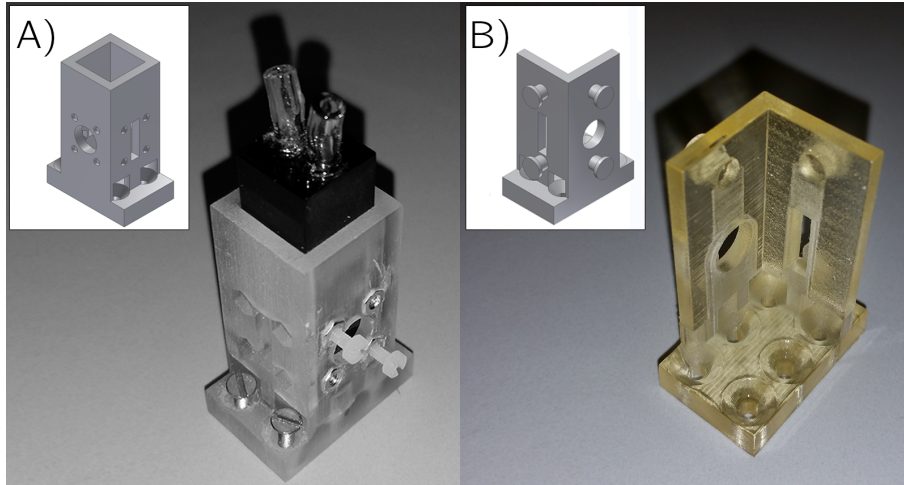


Fig. 3.8: A) Mount design with plastic bolts to fixate the cuvette, B) revised mount to avoid damaging the cuvette during attachment.

Rhodamine B ([9-(2-carboxyphenyl)-6-diethylamino-3-xanthenylidene] - diethylammonium chloride) is a commonly used dye in both cw and pulsed lasers [48]. The dye was chosen because of its good availability and a well known cross section profile (as depicted in 3.9).

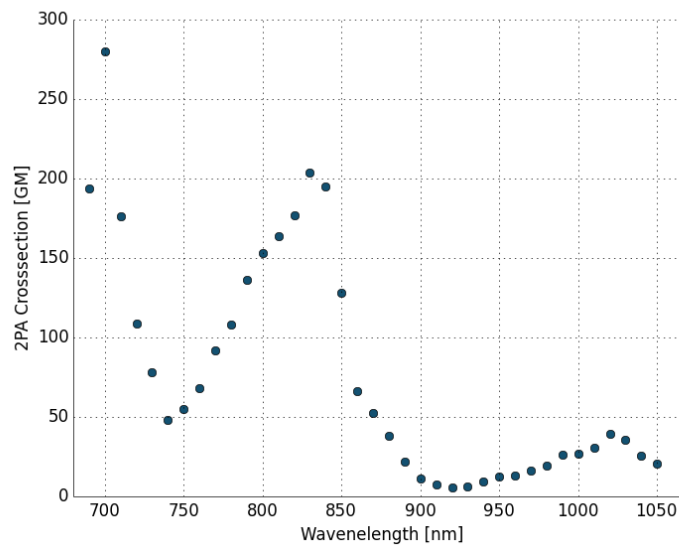


Fig. 3.9: Expected two-photon absorption (2PA) cross section of Rhodamine B. Data taken from [49]

Chapter 4

Results and Discussion

4.1 Waveplate Calibration

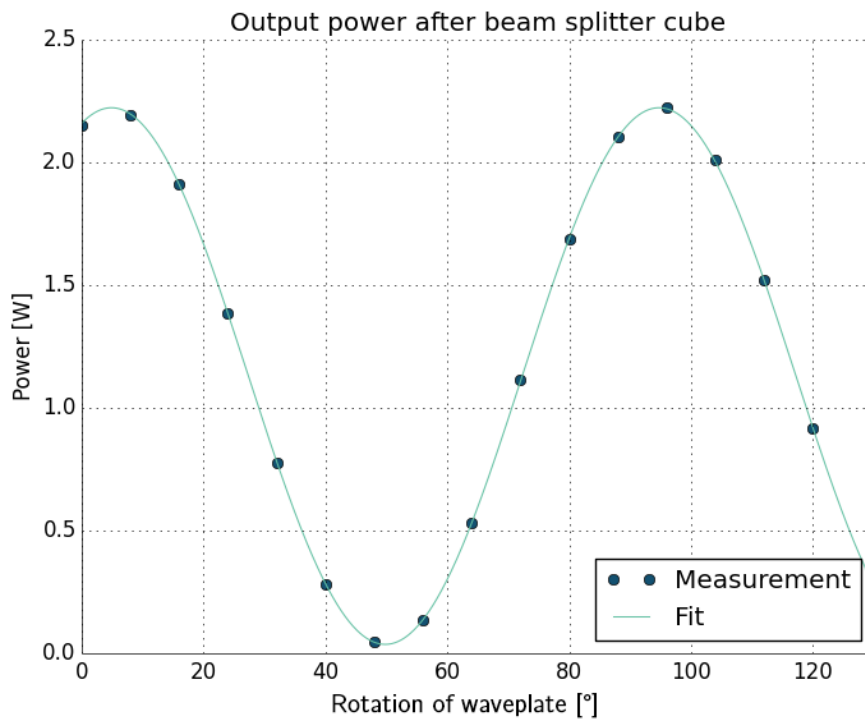


Fig. 4.1: Output power after the beam splitter cube depending on the rotation angle θ of the waveplate at 800 nm.

A program was written to regulate the amount of laser power which was directed into the Z-Scan system. Via a controller (Thorlabs, TSC001), a rotational stage (Thorlabs, PRM1Z8) changed the angle of the waveplate. Using a powermeter (Coherent Inc., Fieldmax II), the output power was measured and read into the

program. Using the angle and power data, the results were fitted according to Eq. 3.1 as displayed in Fig. 4.1.

The program was then used to calibrate the laser system for the wavelength range of the MaiTai in 10 nm steps. From the obtained data a library was compiled which allowed the software to calculate the current laser power by simply reading the angle of the waveplate and the wavelength of the laser. The peak power over the laser spectrum is visualized in Fig. 4.4. The maximum energy is located between 750 and 800 nm. Especially for future multi-wavelength applications, the lower power at the end of the laser spectrum needs to be kept in mind, since an experiment only working for high output powers might yield results for a scanning window around 800 nm, yet not be applicable for lower wavelengths.

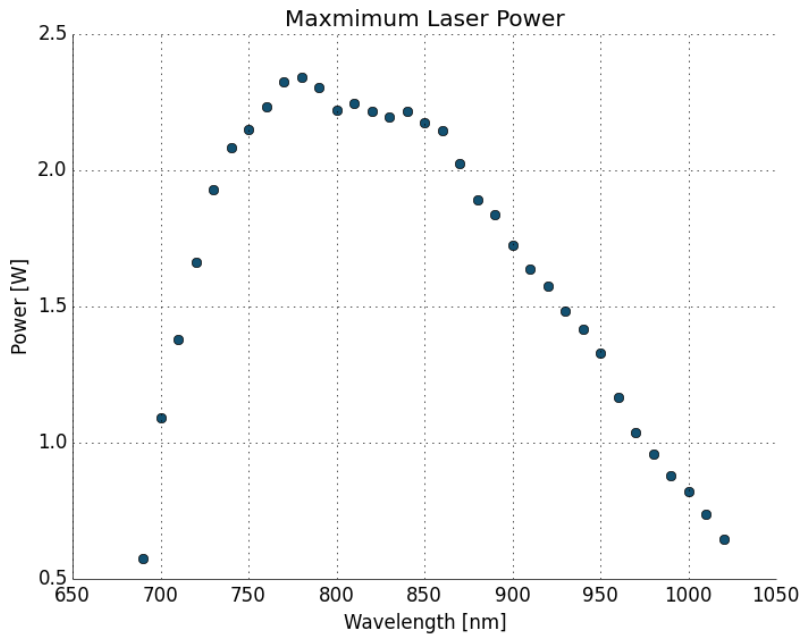


Fig. 4.2: Maximum laser power after the beamsplitter cube (position of waveplate at θ_{max} for all wavelengths).

Also, the transmission to both measurement diodes was observed. The quotient between laser power measured via powermeter and voltage measured by the photodiode was evaluated. These transmissions have to be kept in mind for the sensitivity of measurements at higher/lower wavelengths.

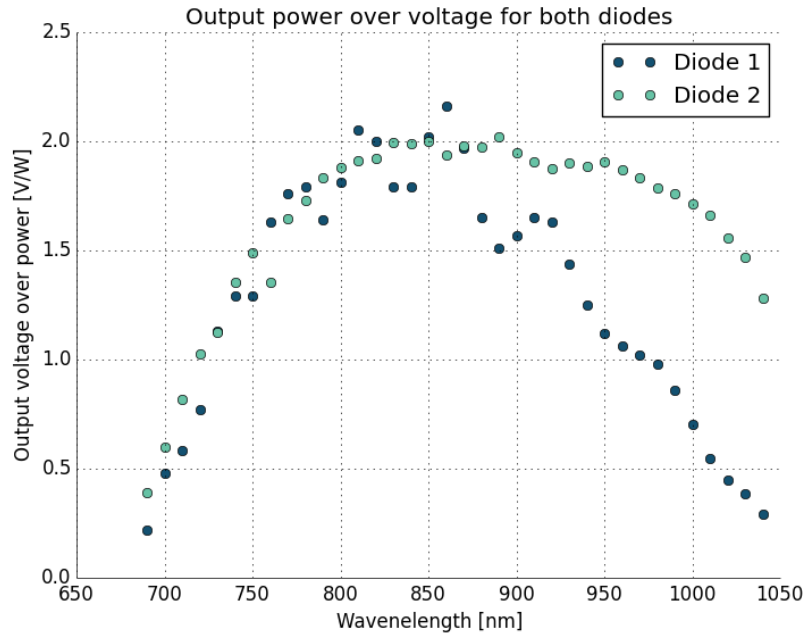


Fig. 4.3: Transmission factor ($\frac{P}{U}$) from after the waveplate (diode 1) and the sample (diode 2). The ratio decreases at both ends of the laser spectrum.

4.2 Power Transmission

With any optical system there are losses at the individual components. The power after each component was measured (see Tab. 4.1) to get an overview of the transmitted intensity. From these results a 75 % transmission at the cuvette was observed. Due to the lower powers used (0.05-0.4 W) in the Z-Scan experiments these losses do not significantly affect the measurements.

Component	Power [W]	T_{rel} [%]	T_{abs} [%]
Emitted from Laser	2.58	100	100
Waveplate	2.51	97.44	97.44
Beam splitter cube (θ_{max})	2.33	92.68	90.31
Beam sampler	2.31	99.14	89.53
Silver mirror	2.16	93.90	84.06
3 Silver mirrors	1.92	88.93	74.76

Tab. 4.1: Measured powers at different positions in the Z-Scan system to evaluate the relative (T_{rel}) and absolute (T_{abs}) transmission after each component. All measurements were done at the maximum transmittance angle θ_{max} of the waveplate.

A second waveplate calibration was done to have an additional library to regulate the power to a certain value before the cuvette. The two libraries could be used

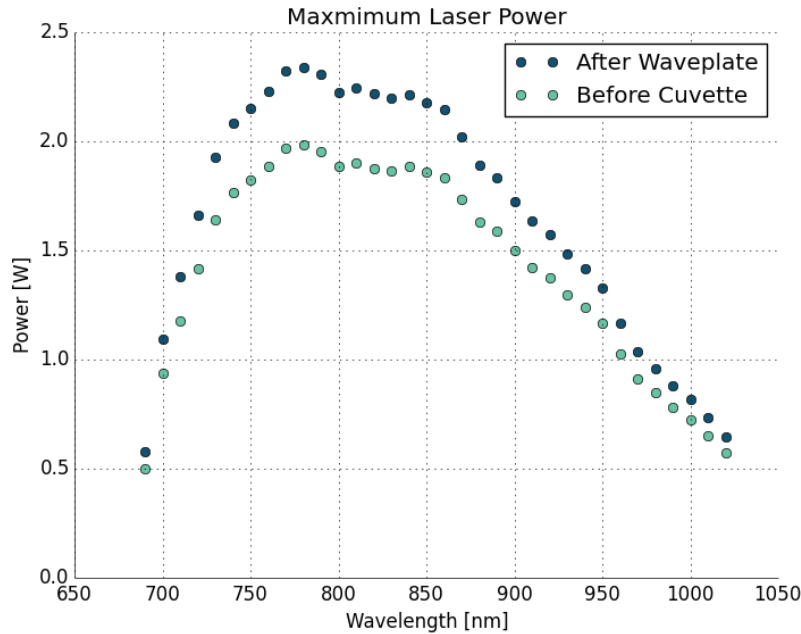


Fig. 4.4: Maximum laser power after the waveplate (θ_{max}) and before the cuvette. Both calibrations allowed to create two libraries to dynamically calculate the laser power for a given angle and position in the experimental setup.

separately, regulating the power either in reference to the cuvette position or the waveplate position. Having two libraries allowed the use of power calibration for other experiments with the MaiTai, which are not related to the Z-Scan setup.

For future calibrations an interpolation algorithm may be used to extrapolate the correct waveplate positions from the given values (for example: use the data from 790 nm and 800 nm to calculate the parameters for 798 nm).

4.3 Beam Profiler

The beam waist ω_0 and the Rayleigh length λ_R are the two parameters needed to fully characterize a laser beam - and significantly play into the Z-Scan (Eq. 2.32). Initially, the Rayleigh length z_R and q_0 (defined in Eq. 2.28) were the two fit parameters for the Z-Scan. However, in the first experiments conducted with the Z-Scan (see Fig. 4.8), the fit returned a z_R of 0.9 mm, which is about 40 % of the actual Rayleigh length at 800 nm for the system. To remove the need to obtain this variable from the Z-Scan data, the beam profiler was considered as a solution to correctly measure z_R .

Due to the sensitivity of the camera optical filters were required to reduce the intensity of the beam when focused onto the camera's chip to record the beam. As

described in Chapter 3.4, a mount was designed and printed to fit the camera onto the stage (Fig. 3.2). For each stage position the beam data was collected and fitted as shown in Fig. 4.5.

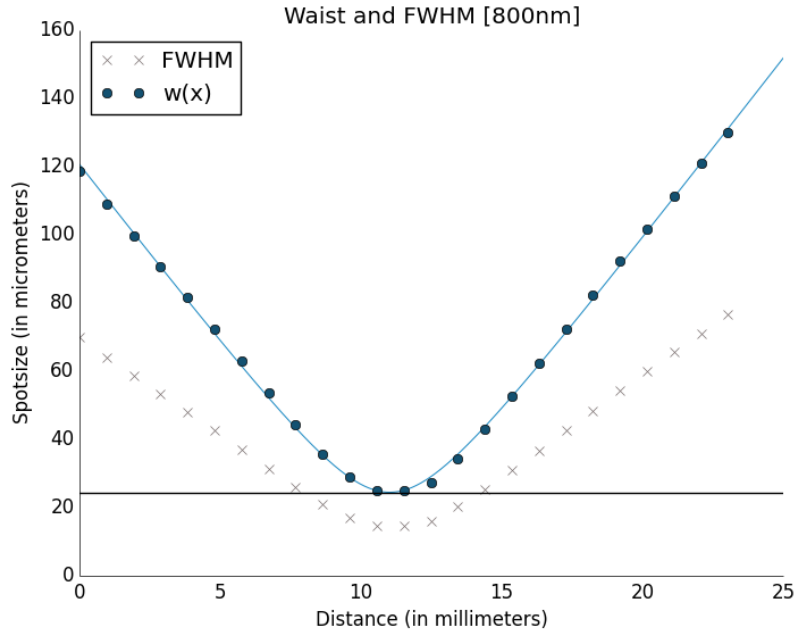


Fig. 4.5: Comparison between FWHM and Waist with the theoretical fit at 800 nm. Horizontal line shows ω_0 .

Since the initial setup contained a refractive expander running the experiment for different wavelengths and therefore caused a shift in focal distance in dimensions of millimeters (see Tab. 4.2). This effect was traced back to chromatic aberration (as discussed in Chapter 2.4.4). A scanning distance of $z_0 \pm 5 \cdot z_R$ is necessary to get sufficient Z-Scan data [11]. With z_R in the range of 2 mm this meant that the 25 mm length of the stage used was sufficient for the scanning distance. However, a shift of 6.63 mm at 1000 nm would have required scanning range outside of the stage's distance.

λ	690	700	730	780
Δz_0	-5.01	-4.59	-2.92	-0.34
λ	850	900	950	1000
Δz_0	2.46	3.13	1.89	6.63

Tab. 4.2: The relative focus shift to the focal position at 800 nm for the refractive expander was up to 6.63 mm which would place the required scanning distance $z_0 \pm 5 \cdot z_R$ outside of the stage's distance.

This would have necessitated a manual adjustment of the stage for each individ-

ual wavelength, which would have run counterproductive to the project's intention. Consequently, the refractive beam expander was replaced by a reflective one, which meant realigning the beam path (seen in Fig. 3.6) as discussed in Chapter 4.4.

After this readjustment the beam profiling was repeated with the reflective expander. The focal plane was stable in a tenth of the refractive results from the reflective expander (see Fig. 4.7). The new alignment was feasible for automated multi-wavelength scans. The data collected can be seen in Tab. 4.3.

λ [nm]	ω_0 [μm]	z_R [mm]	z_0 [mm]	Δz_0 [mm]
690	29.1	3.55	11.30	0.28
700	26.6	3.23	11.67	0.65
720	25.8	2.91	11.36	0.34
740	26	2.84	11.26	0.25
760	25.3	2.7	11.10	0.08
780	24.8	2.4	11.08	0.06
800	24.5	2.28	11.02	0.0
820	23.3	1.99	10.96	-0.06
840	24.3	2.04	10.84	-0.17
860	23.8	2.02	10.69	-0.32
880	24.9	2.14	10.80	-0.21
900	26.1	2.2	10.78	-0.23
920	26.4	2.28	10.73	-0.28
940	23.9	2.07	10.72	-0.29
960	23.9	2.07	10.72	-0.29
980	25.4	2.25	10.80	-0.21

Tab. 4.3: Results for different wavelengths λ using the reflective expander. The shifts in z_0 are notably lower compared to the results from the setup with the refractive expander.

The profiling became less reliable for higher wavelengths in the infrared spectrum as the uEye chip's quantum yield decreased for IR-light. Increasing the intensity led to measurable data. The experiments were conducted close to the minimum laser power to prevent damaging the camera's chip and the filters.

For the initial profiling, absorptive neutral density (ND) filters were used to evenly reduce the intensity profile, to protect the camera chip and the reference diode. These absorptive filters were chosen to avoid reflections into the laser system. Since multiple filters were damaged over the course of the Z-Scan (see Fig. 4.6 B) the absorptive filters were replaced by reflective filters. Wedged filters were chosen to avoid reflection into the system.

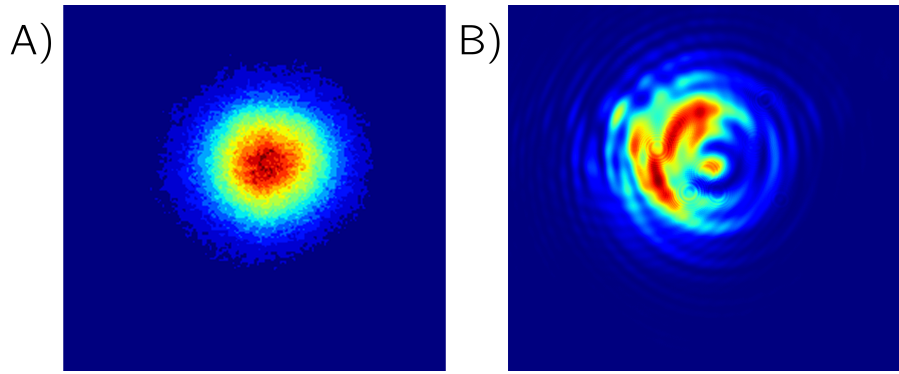


Fig. 4.6: A) regular beam profile, B) beam profile with damaged filter.

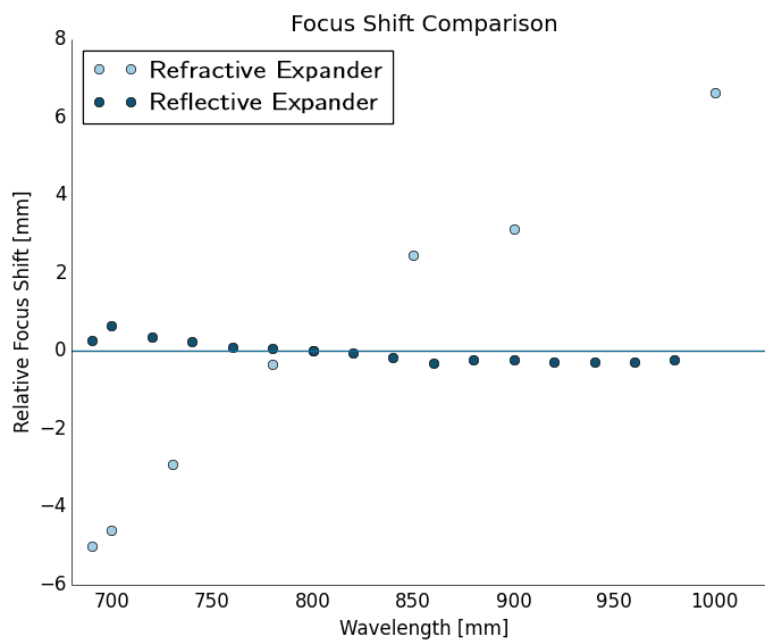


Fig. 4.7: The relative shift in focus position (800 nm position used as zero position) for both expanders clearly shows the smaller fluctuation in z_0 for the reflective expander.

4.4 Z-Scan

4.4.1 Continuous Z-Scan

The initial Z-Scans of Rhodamine B and an average laser power of 0.4 W at the sample (the waveplate calibration had to be done in front of the sample due to the losses in transmission of the laser system as discussed in Chapter 4.2).

Additionally, the material was pumped through the cuvette using a motorized pump operated at different flow speeds, as photodegradation and higher ordered absorptions can distort the measurement [50].

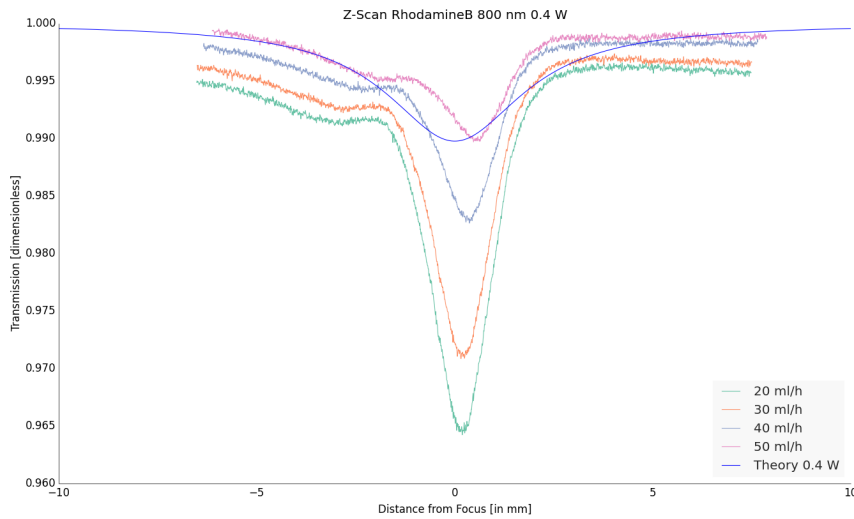


Fig. 4.8: Z-Scan for different flows at 0.4 W yielded significantly higher absorption than the theory (blue line) predicted. Theoretical plot with $\sigma_2 = 150$ GM and $z_0 = 2.1$ mm.

As can be seen in Fig. 4.8, the absorption was much larger than the theory predicted. These results were crucial in motivating the beam profiling Chapter 4.3 since both q_0 and z_R were initially obtained from the fit. Yet for the fit to match the results, a Rayleigh length in the range of 0.9 mm would have been necessary to get the steep drop of the observed graphs.

The beam profiler (Chapter 4.3) allowed to conclude that the observed results were not due to 2PA, but to other processes like thermal absorption.

After the beam profiling, the experiment was repeated at 0.2 W, again with alternate flows through the cuvette (see Fig. 4.9). Yet no q_0 could be found to adequately fit the results. The extracted cross section values from both experiments can be seen in Tab. 4.4. While the results for 0.2 W and 30 ml/h were close to the cross section values from literature [49], it must be noted that the function could not be adequately fitted to the measurement using this parameter. Therefore,

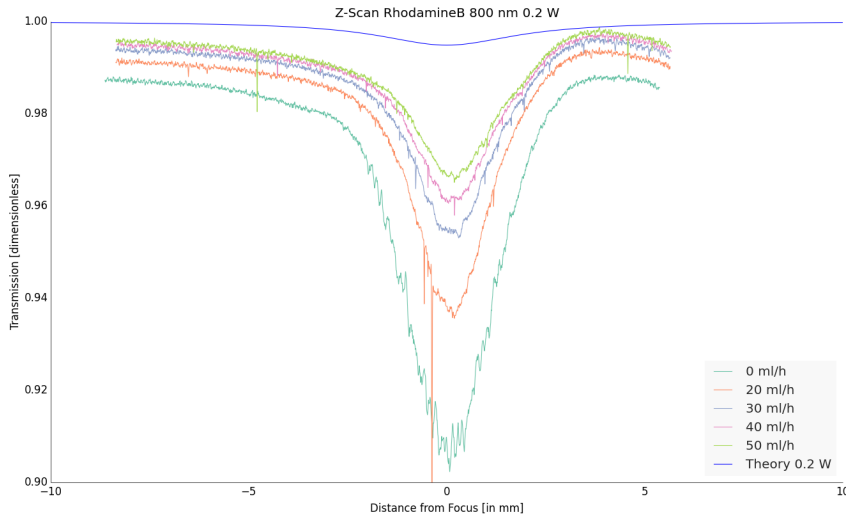


Fig. 4.9: Z-Scan for different flows at 0.2 W.
Theoretical plot with $\sigma_2 = 150$ GM and $z_0 = 2.1$ mm.

the fit results were close to the theory, but did not adequately describe the actual measurements. Similarly reduced cross section for increased flow ran against the expected behavior. Increased flow reduces photo degradation effects and should yield a higher cross section [34]. This implies that the flow through the cuvette acted as a coolant for the sample and reduced the thermal absorption behavior.

Extracted cross sections [GM]		
Flow [ml/h]	0.4 W	0.2 W
0	130.8	361
20	100.8	202
30	81.3	157.2
40	49.4	132.7
50	32.2	117

Tab. 4.4: Cross sections for experiments at 0.4 W and 0.2 W.
While the calculated value for 0.2 W and 30 ml/h corresponded to the theory,
it did not accurately describe the actual measurement.

Since the increased flow led to curves closer to the predicted theory, the laser power was further reduced to 0.15 W (Fig. 4.10) and 0.13 W (Fig. 4.11). Especially, the scan at 0.13 W showed a strong asymmetric behavior of the transmission, where it should have been a completely symmetric curve for open aperture scans [19].

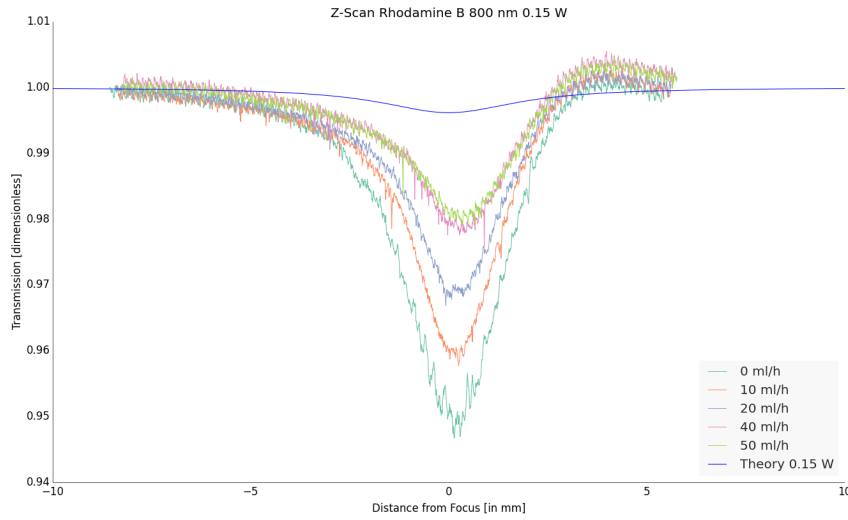


Fig. 4.10: Z-Scan for different flows at 0.15 W. Increased flows yielded results closer to the theory, yet there was still a steep drop. Theoretical plot with $\sigma_2 = 150$ GM and $z_R = 2.1$ mm.

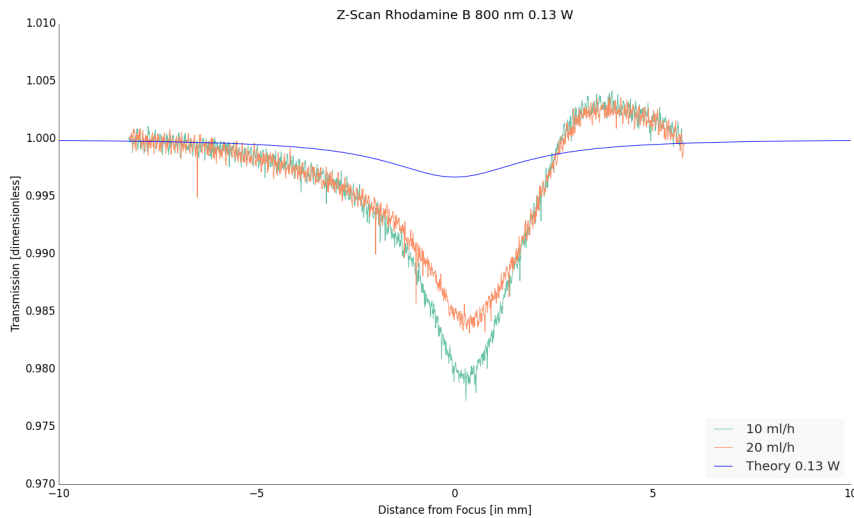


Fig. 4.11: Z-Scan for different flows at 0.13 W. For this lower power measurement, increasing the flow beyond 30 ml/h did not return measurable results. The results also showed a clearly asymmetric behavior uncharacteristic for the Z-Scan, which should be symmetric for open aperture scans. Theoretical plot with $\sigma_2 = 150$ GM and $z_R = 2.1$ mm.

Again, the cross sections extracted from the fit decreased with increasing flow even below the reference value of 150 GM (results in Tab. 4.4). Similarly to the measurements at higher powers, there was a problem with the accuracy of the fit, since the observed loss in transmission signal was still much sharper than the theory suggested. With increased flow, the obtained data were also less reliable due to the transmission signal drop in similar order of the background noise. This rendered a

measurement for 40 ml/h and 50 ml/h at 0.13 W which was too inaccurate for a sufficient fit.

Extracted cross sections [GM]		
Flow [ml/h]	0.15 W	0.13 W
10	160	86
20	126	69
30	no data	67.5
40	93	no data
50	85.9	no data

Tab. 4.5: The observed cross section decreased for higher flows.

For 40 ml/h and 50 ml/h at 0.13 W the measured data were insufficient for reliable fitting.

4.4.2 Lower Power Limit

After observing a trend of results closer to theory for higher flow speeds and lower power, another experiment for Rhodamine B was initiated: At a constant speed of 40 ml/h the power was reduced in 10 mW steps until the drop in transmission could no longer be observed. This was done to decrease the effects of thermal lensing and photo degradation. The scan was then repeated for the last observable drop (0.05 W) as the measurement was affected by the background noise (standard deviation of ± 39.9 GM).

The very low power and consequent lower drop in transmission made the signal evaluation much more difficult. The high noise had to be averaged for visual representation (Fig. 4.12).

The observed cross section values for Rhodamine B, which did not match the expected cross section of 150 GM, are gathered in Tab. 4.6.

Power[W]	Cross section [GM]
0.1	335
0.07	205
0.06	258
0.05	220 ± 39.9

Tab. 4.6: The laser power was lowered in 10 mW steps until no more observable drop was recorded. For the limit of 0.05 W multiple measurements were taken since the small drop in signal caused high uncertainties in the measurements.

Reducing the laser power was no longer an option, as at powers lower than 0.05 W the signal was overlaid with background noise and could no longer be reliably

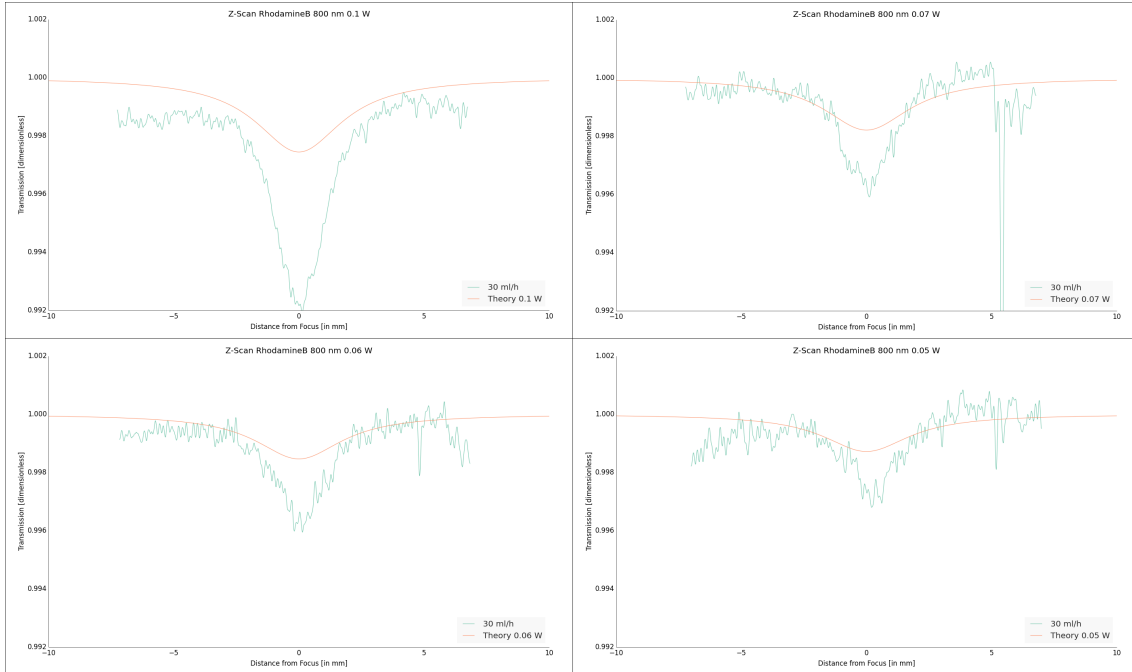


Fig. 4.12: Z-Scan for lower powers. While yielding results closer to theory, the measurements were also susceptible to high noise. For visual depiction the noise was averaged. Theoretical plot with $\sigma_2 = 150$ GM and $z_R = 2.1$ mm.

observed. In addition, the high flow speed presented an implementation problem: flow speeds of 40 ml/h would require a huge amount of substance necessary to record a single Z-Scan, making this method less feasible for expensive substances and multiple scans.

From the conducted experiments, an interesting behavior was observed, since the increased flow yielded lower absorption. Yet, as shown by research in literature [51], the absorption should increase for higher flows, as a static liquid is susceptible to photo degradation. Therefore, longer exposure of a resting liquid should exhibit less reactive material which is able to absorb the incoming light.

Because of these observations, it was concluded that thermal lensing [32, 34] might have been the cause for the increased absorption. Since the thermal diffusion coefficient of Rhodamine B is $4.5 \cdot 10^{-3} \frac{\text{cm}^2}{\text{s}}$ [52] and the repetition laser's rate is 80 MHz, the characteristic time (Eq. 2.50) was too long for the sample to return to the equilibrium state. This heating of the sample caused laser-induced density and refractive index gradients, which in turn lead to a focusing effect (thermal lensing). The material acted as an additional lens. A solution using a beam chopper was devised, in order to decrease the effect of thermal heating.

4.4.3 Beam Chopper Mode

A custom-built beam chopper (rotation frequency of 3000 Hz) was placed before the beam expander to reduce the exposure time of the sample. To quantify the data, the software reading the diode data had to be modified. The oscilloscope was triggered by the pulsed signal, thus only taking measurements the pulse signal passed a predetermined threshold. Previously, the oscilloscope data had continuously been extracted while the sample had been moved through the beam. Triggering the oscilloscope to the flank of the pulsed signal allowed a closer look at the signals of the reference diode (D1) and measurement diode (D2). Therefore, a reflection of the laser beam was observed when the sample was moved into the laser focus (as seen in Fig. 4.13). A part of the beam was reflected by the cuvette and traversed the path right back to the first diode, therefore diluting the reference signal.

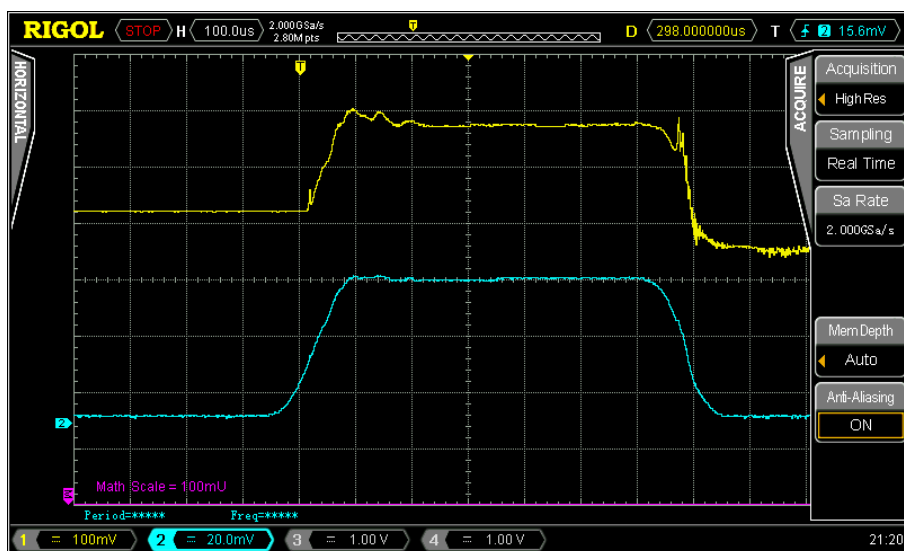


Fig. 4.13: Reflected signal at reference diode (D1, yellow) when the sample was moved into focus. Since the reference signal should be a stable line since it is used to normalize the measurement signal (D2, blue). If the reference signal increases for the focus the increased denominator D1 in $(D2/D1)$ causes a smaller ratio at the focus and therefore an even larger drop.

For each position the signal of the measurement diode (D2) was normalized by the reference signal (D1), which should have been stable for all measurements. An increase in (D1) near the focus changed the denominator in $D2/D1$ so the normalization was no longer a constant. It affected the results by an even larger drop at the focus in addition to the thermal absorption. Slightly changing the angle of the cuvette mount (which was previously placed perpendicular to the incoming beam) enabled a clear reference signal. The issue faced was the fact that tilting the cuvette narrowed the surface exposed to the beam. With a cuvette window of 1 mm, the target area was reduced so that even a slightly incorrect laser beam was truncated

by the sample holder. To make the setup less susceptible to errors in the beam path, a cuvette with a wider window (2 mm) was chosen. The new cuvette had a sample thickness of 0.2 mm, thus requiring higher beam intensities (smaller L_{eff} in Eq. 2.32). The experiments with this cuvette were conducted at 1.9 W. The beam chopper setup was able to record and plot the transmission for varying flows with a clear reference signal (see Fig. 4.14).

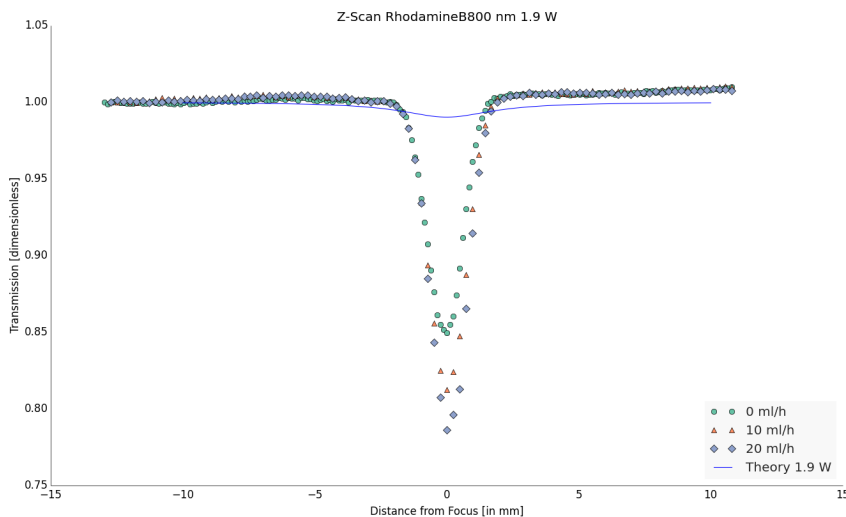


Fig. 4.14: Z-Scans at 1.9 W with alternate flows. Increased flow resulted in higher absorption due to less photo degradation.

The observed absorption was still larger than the theory predicted. Contrary to the continuous scan method, increasing the flow also increased the absorption until the effects of photo degradation were reduced [51]. The signal transmitted to the oscilloscope was monitored for different laser intensities (1 W, 1.7 W, 1.9 W) and varying sample positions. As can be seen in Fig. 4.15, there was an increased signal drop for higher laser powers at the focal position (13 mm in this experiment). This drop was notably lower for 1.7 W and vanished for 1 W. These observations lead to the assumption that for powers lower or equal to 1 W the off-time caused by the shutter was enough to observe steady data while still avoiding thermal effects. The drop in signal for higher powers was probably due to the sample heating as observed in the previous experiments. Since the program took the mean over the entire wavefront, it can be seen why the signal drop was so high at 1.9 W compared to the predicted theory.

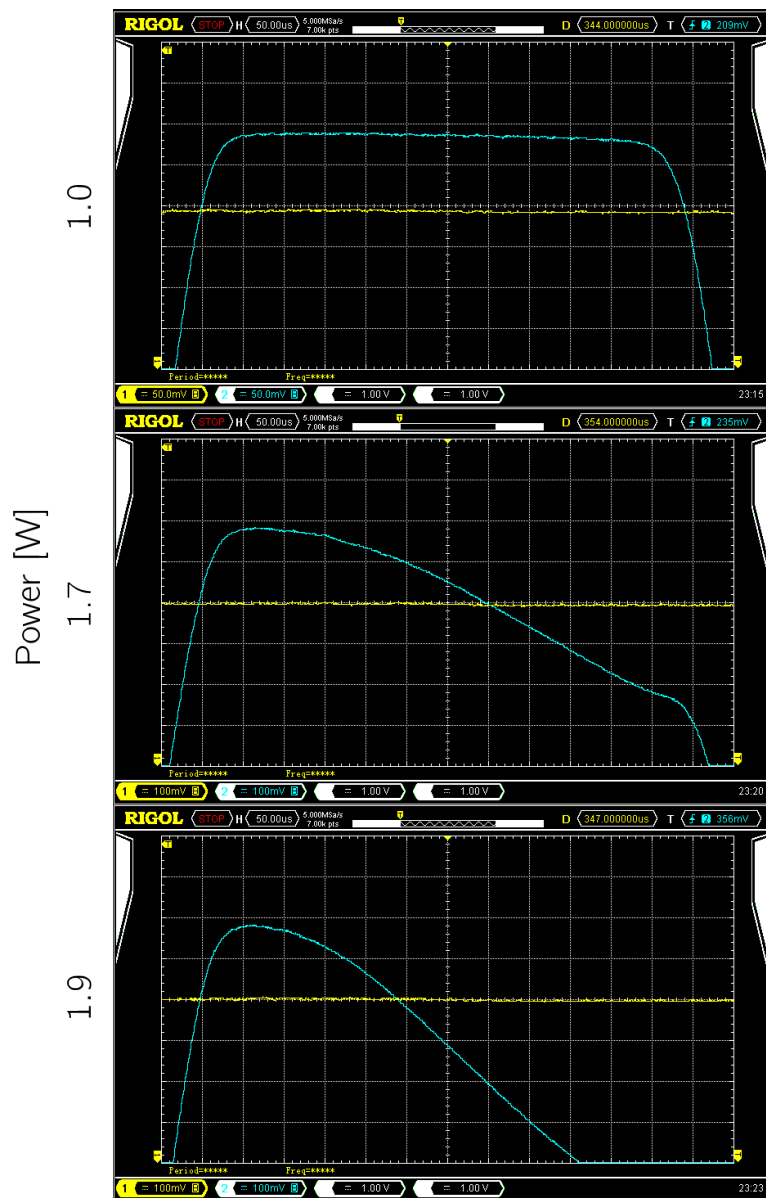


Fig. 4.15: Measured signal (D2, blue) for different powers at the focus position (13 mm). A drop in signal over time was observed at 1.7 W and 1.9 W. This drop did not occur for 1.0 W, which leads to the assumption that it is a drop caused by thermal effects.

Chapter 5

Conclusion

A multi-wavelength beam profiler has successfully been implemented which allows reliable extraction (and control) of the beam parameters for different wavelengths. The thermal effects have been reduced by installing a beam chopper and triggering the diodes to the flank of the signal.

In the initial setup higher flows of material yielded less absorption behavior. This may be linked to the flow acting as a coolant for the sample, therefore reducing the thermal effects, and the absorption mechanisms they cause.

With the new setup the absorption increases for higher flow speeds. This corresponds to the theory that a flow of fresh material reduces the effects of photo degradation.

For the new setup a cuvette with a larger window (6.5 mm) was used enabling the tilting of the cuvette to avoid reflections back into the laser system. This second cuvette was thinner (0.2 mm) than the initial one (1 mm), which required laser power to observe 2PA. This high power was again responsible for thermal heating which can be observed over the duration of the pulse.

To solve this heating problem we suggest to increase the optical path of the beam through the material, therefore decreasing the required intensity.

Chapter 6

Supplements

Over the course of this project an interface was written to access the various components (MaiTai, rotating waveplate, uEye camera). In this section, the functions of the interface are elaborated. Later various methods are described and illustrated by selected segments of code. The project was written in Python 2.7.

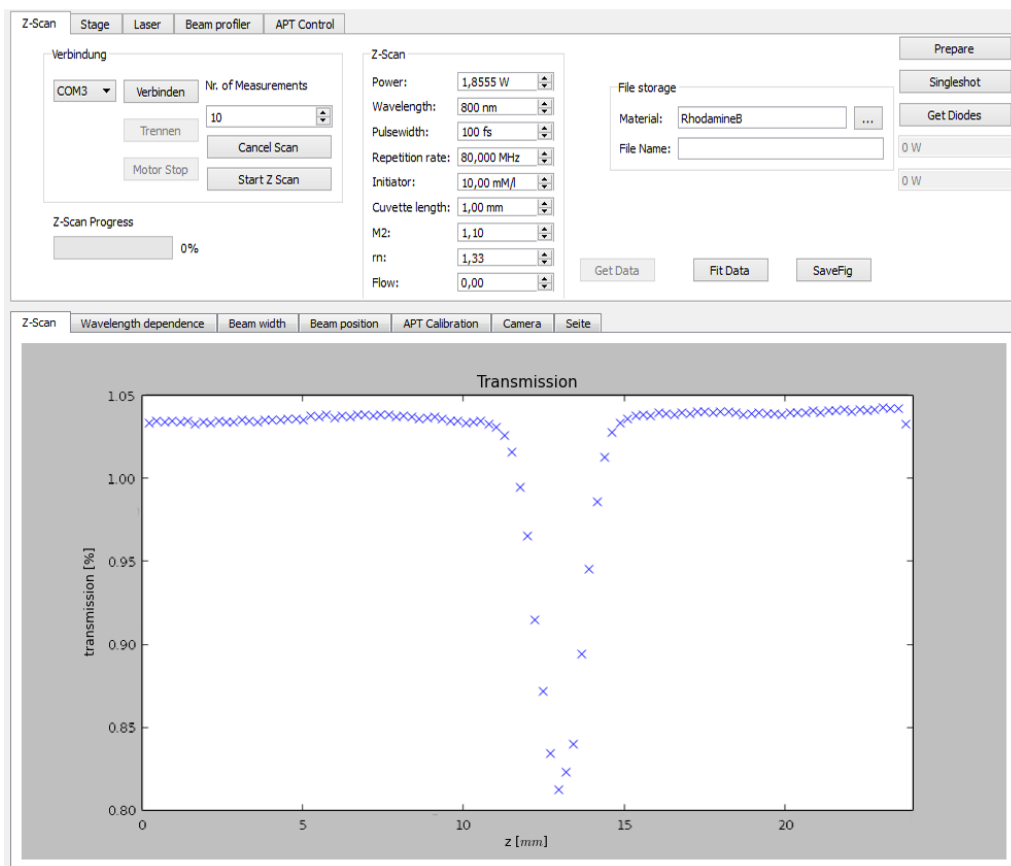


Fig. S1: Main interface for the Z-Scan. The “number of measurements” determines the amount of equidistant points along the stage.

Interface

The main GUI for the Z-Scan (Fig. S1) allows the user to connect to the oscilloscope via COM port and start the Z-Scan. The parameters can be entered into the textbox in the label “Z-Scan”. These values are also accessed by the algorithm to fit the cross section (see Chapter 6). The textbox “materials” designates the folder where the data is stored. Individual measurements can also be loaded. The filename for the measurements is automatically generated using the date (yyyy-mm-dd), time (hh-mm), material, wavelength (nm), concentration (mM/l), laser power (W) and flow speed (ml/h). The buttons “Prepare”, “Singleshoot” and “Get Diodes” are functions which enable single measurements by the oscilloscope. The Z-Scan is initiated by the button “Start Z-Scan” which moves the sample to a number of equidistant positions along the stage to measure the signal at the diode (D2). While a software to access the MaiTai laser was provided, a program was written to implement the commands for the laser (given by the MaiTai manual [53]) into the GUI (see Fig. S2). When started, the program tries to connect with the laser via COM port.

If the laser has been connected, the user can switch the laser on and off and change the shutter status. The wavelength of the laser can also be changed by the user. The program dynamically reads the laser power from the MaiTai to visualize it on the right side of the tab.

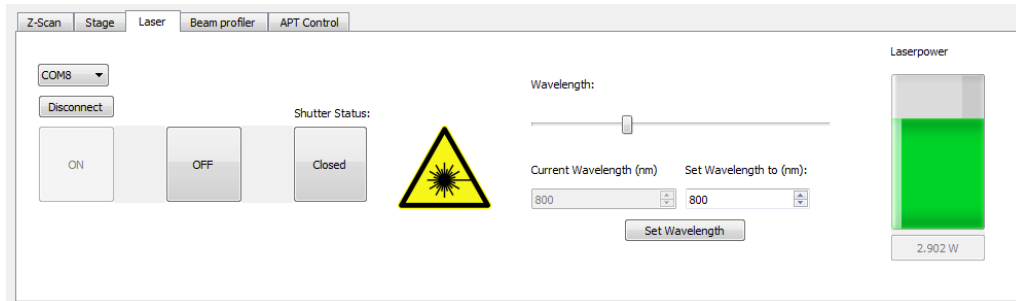


Fig. S2: Tab for the MaiTai Laser which attempts to connect at the program’s start. The laser power is continuously read and displayed.

If for some reason automatic connection failed upon start the disconnect/connect button allows manual connection. Upon exiting the program the shutter is automatically closed to guarantee laser safety and the user is asked if the laser should be turned off as well.

The tab “APT Calibration” accesses the rotational stage [54] to change the waveplate’s angle (Chapter 4.1) and read the power from the powermeter for the given rotation. The number of measurements by the user determines the equidistant shifts in rotation angle from 0 to 120 degrees. If a library for the laser’s selected wavelength exists the Spinbox “Set Laserpower” automatically calculates the laser

power based on the current rotational angle. It enables the user to enter the desired laser power. The button “Set Laserpower” then calculates the required angle from the library and rotates to this position. The connection to the rotational stage is established automatically upon the program’s start, yet it can be enabled/disabled manually by the user. When running the calibration the data is dynamically plotted into the bottom window. After all measurements are finished and the curve fit has been successful, the theoretical plot is added to the measurements.

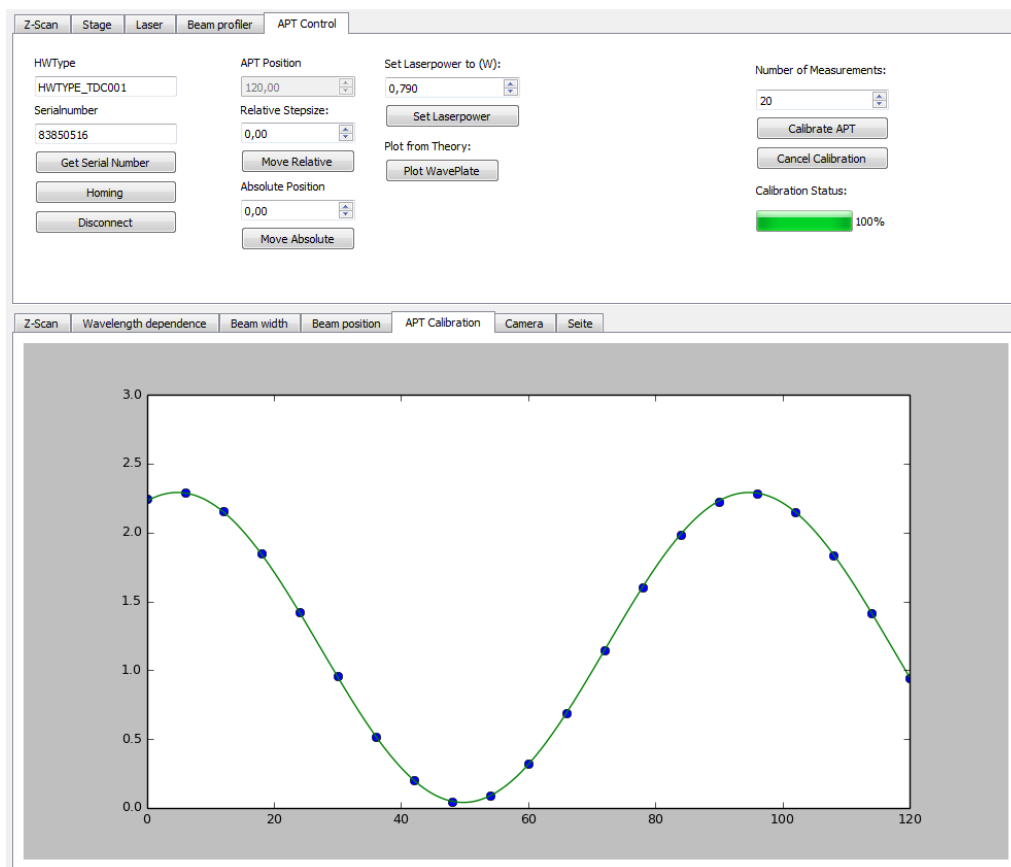


Fig. S3: This tab allows to calibrate the output powers for different waveplate angles. The results are plotted for each measurement (number of measurements selected by user) and the theoretical fit obtained from the data is plotted after the process is finished.

Under the tab “Stage” (Fig. S4) the LCS16-025-2(4)5 can be moved to any position at the desired speed. Specific commands can be read and sent to the SMAC controller as well [55].

In the tab beam profiler (Fig. S5) the button “Start Profiling” moves the stage to a number of equidistant measurement positions which are determined by the user. At each position, the program accesses the uEye camera to record the laser beam.

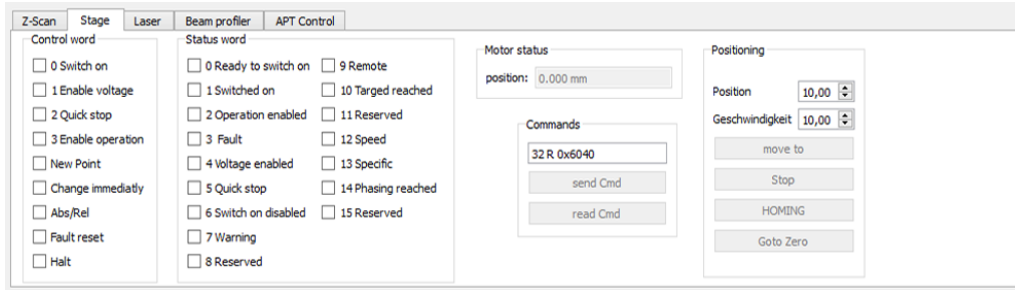


Fig. S4: The position of the stage is continuously read and updated. The user can either enter specific commands or move the stage to a desired position at a given speed.

For each position z the waist $\omega(z)$ is calculated and plotted. After all the measurements are done the widths are fitted using Eq. 3.4 and plotted. The extracted beam waist ω_0 is displayed in the spinbox on the top right side. This value is also used by the Z-Scan program to fit the cross section.

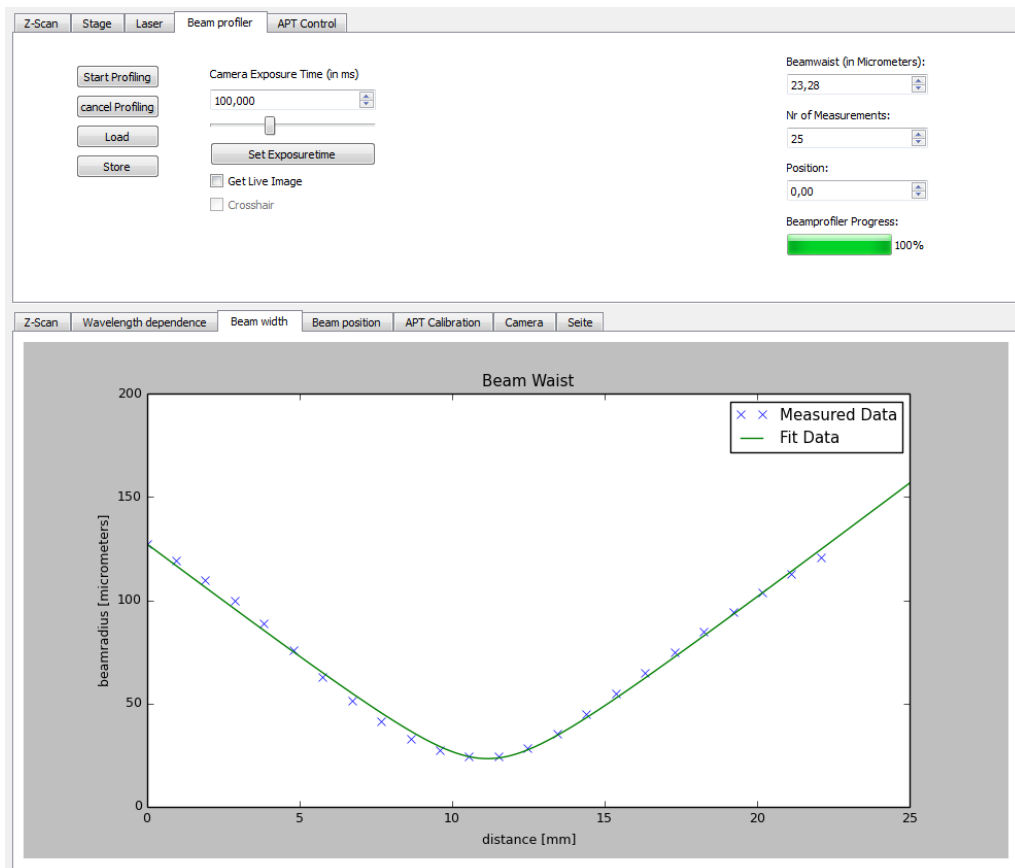


Fig. S5: The camera's exposure time is determined by the user and continuously reduced if the sensor is overexposed. The measured beam widths $\omega(z)$ are plotted along with the fit.

If the beam profiler is not running, the camera can also be accessed to get a live image by clicking the checkbox. An additional crosshair can be added to the live image to aid the centering of the beam path. The camera's exposure time can

be adjusted and the program uses this value for the initial settings. If the image reduction algorithm finds a white pixel (value= 255), the chip is overexposed and the program continuously reduces the exposure time by a third until no white pixels are detected. With this method, the program ensures that the Gaussian distribution is always recorded correctly without the need for manual readjustment.

MaiTai

Based on the commands protocols for the MaiTai [53], the laser was accessed via COM port. The MaiTai class initializes the laser and reads the laser parameters. An important paramter to set is the `Watchdog` which has to be set to 0. Otherwise the MaiTai will switch off and disconnect after 1 second.

Source Code

```
1 import serial
2
3 class MaiTai():
4     def __init__(self):
5         """ create serial connection """
6         print "init Laser"
7         self.ser = serial.Serial()
8         self.isLaserOn = False
9         self.isShutterOpen=False
10        self.wavelength=800
11        self.laserpower=0
12        #watchdog needs to be set to 0
13        #otherwise the MaiTai will automatically switch off
14        #after 1 sec
15        self.Watchdog(0)
16
17    def connect(self , COM):
18        """
19        connects to the controller over the given serial port
20        return: True if connected , else False
21        """
22        #print "connect to index " + str(port) + " as " + self.
23        #COM_portlist.itemText(port)
24        if not self.ser.isOpen():
25            print "open COM-Port: " , COM
```

```
24         try:
25             self.ser = serial.Serial(port=str(COM), baudrate
26                                     =9600, timeout=0.2) # open first serial port
27         except serial.serialutil.SerialException:
28             #port already used
29             self.ser.close()
30             return False
31
32         print self.ser
33         print self.ser.portstr          # check which port was
34                                         really used
35     #try to talk to the controller if he is really
36     responding
37     self.ser.write("*IDN?\r")
38     rec = self.ser.readline()
39     print "ID: %s" %rec
40     if rec=='':
41         #device not responding - shut down connection
42         self.ser.close()
43         return False
44     self.Watchdog(0)
45     self.getWavelength_int()
46     return True
47 #connection already opened
48 return True
49
50 def disconnect(self):
51     #disconnectes the connection between LCC-controller and
52     PC
53     #return: False if disconnected
54
55     if self.ser.isOpen():
56         print "disconnect Laser"
57         self.ser.close()
58
59 def on(self):
60     if not self.ser.isOpen():
61         return
62     if not self.iswarmedup()==100.0:
63         print "can't start laser because it is not warmed up
64             "
```

```
60         return -1
61     print "turn Laser on"
62     self.isLaserOn = True
63     self.ser.write("ON\r")
64
65     def off(self):
66         if not self.ser.isOpen():
67             return
68         print "turn Laser off"
69         self.isLaserOn = False
70         self.ser.write("OFF\r")
71
72     def iswarmedup(self):
73         if not self.ser.isOpen():
74             return
75         self.ser.write("READ:PCTWarmedup?\r")
76         rec = self.ser.readline()
77         print rec
78         laser_warmed=float(rec.replace("%", ""))
79         if laser_warmed==100.0:
80             print "Laser Warmed up"
81             return 100.0
82         else:
83             print "Laser not yet warmed up. Status: %f" %
84                 laser_warmed
85             return laser_warmed
86
87     def setShutter(self, enable):
88         if not self.ser.isOpen():
89             return
90         enable = bool(enable)
91         print "enable shutter: %s" % enable
92         self.ser.write("SHUTter %i\r"%enable)
93         self.isShutterOpen = enable
94
95     def getShutter(self):
96         if not self.ser.isOpen():
97             return
98         #empty buffer
99         #self.ser.readline()
```

```
100
101     self.ser.write("SHUTter?\r")
102     rec = self.ser.readline()
103     return bool(rec)
104
105     def getWavelength(self):
106         if not self.ser.isOpen():
107             return "800.0nm\n"
108         self.ser.write("READ:WAVelength?\r")
109         rec = self.ser.readline()
110         #rec=rec.replace("\n","")
111         #self.wavelength=rec
112         return rec
113
114     def setWavelength(self, wavelength):
115         if not self.ser.isOpen():
116             return
117
118         self.ser.write("WAVelength %s\r"%(wavelength))
119
120         rec = self.ser.readline()
121         self.wavelength=wavelength
122         #print "Wavelength set to: %s" %rec
123         return rec
124
125     def getPower(self):
126         if not self.ser.isOpen():
127             return
128         self.ser.write("READ:PLASer:POWer?\r")
129         rec = self.ser.readline()
130         #print "Laser Power %s" %rec
131         return rec
132
133     def getOutputPower(self):
134         if not self.ser.isOpen():
135             return
136         self.ser.write("READ:POWer?\r")
137         rec = self.ser.readline()
138         #print "Laser Power %s" %rec
139         #print rec
140         return rec
```

```

141
142     def Watchdog(self ,time):
143         if not self.ser.isOpen():
144             return
145         #self.ser.write("TIMER:WATCHdog 0\r")
146         self.ser.write("TIMER:WATCHdog %i\r"%time)
147         rec=self.ser.readline()
148         print "Watchdog message",rec
149         return rec

```

Waist

This algorithm was used to fit the beam width $\omega(z)$ (Eq. 3.4), extract the Rayleigh length z_R and the beam waist ω_0 from the image fitting (algorithm see Chapter 6). The data arrays for the functions have to be of the format

$$data = [I_0, x_0, y_0, \sigma_x, \sigma_y, d]$$

with the peak intensity (I_0), the center positions (x_0, y_0), the widths (σ_x, σ_y) and the sample position (d). As the results from the image analysis are given in pixels, the function `cleanup_data` serves two purposes: It checks if any measurements are of type NAN or above a defined threshold (in this case $\omega(z) \geq 200$) by creating a mask of 0s (keep measurement) and 1s (discard measurement). Secondly, after the mask is applied to the measurement data, the pixels are converted to μm or (in the case of the stage distance) mm by using the `px_to_micrometer` conversion factor.

After this procedure `calculateW0` is used to fit the data and extract the beamwaist ω_0 .

Source Code

```

1 import matplotlib.pyplot as plt
2 from scipy.optimize import curve_fit
3 from numpy import *
4
5 class Waist(object):
6     def __init__(self):
7         self.px_to_micrometer=2.2 # ratio for camera
8         self.data=0
9         self.beamwaist=20
10        self.beamfocus=12000
11        self.rayleigh_length=2300

```

```

12
13     def w(self , z , w0 , z0 , zmin) :
14         return w0*np.sqrt(1+((z-zmin)/z0)**2)
15
16     def create_mask(self , array) :
17         # this function checks if there
18         # are NAN values in the array
19         # it also checks if the measured
20         # value is above a threshold
21         # (200 microns)
22
23         mask=np.zeros(array.size)
24
25         for i in xrange(0,array.size):
26             if np.isnan(array[i]):
27                 print "ISNAN!"
28                 mask[i]=1
29             if array[i]<0:
30                 mask[i]=1
31
32             if array[i]>200:
33                 mask[i]=1
34
35         return mask
36
37     def cleanup_data(self , data) :
38         # converts pixels to micrometers
39         # and mm before the results
40         # are sent to the GUI
41
42         if data.size==0:
43             print "array is empty"
44             return []
45         if data.size==6:
46             return data
47
48         px_to_micrometer=self.px_to_micrometer
49         # widths_x=data[:,3]
50         mask=self.create_mask(data[:,3])
51
52         cleandata=np.zeros(data.shape)
53         for i in xrange(0,6):
54             cleandata[:,i]=ma.array(data[:,i], mask = mask).

```

```

        compressed()
48     if i==5:
49         cleandata[:,i]=data[:,i]*1e3 # #1e3 to switch
           from mm to micrometers
50     else:
51         cleandata[:,i]=data[:,i]*self.px_to_micrometer
52     return cleandata
53
54     def calculateW0(self, data):
55         widths_x=data[:,3]
56         distances=data[:,5]
57         waist_x=2*widths_x # standard gauss distribution
58
59         popt, pcov = curve_fit(self.w, distances, waist_x, p0
           =[50,15000,1000])
60
61         w0=popt[0]
62         z0=popt[1]
63         zmin=popt[2]
64
65         wavelength=np.pi*w0**2/z0
66         print "Wavelength = ", wavelength, " micrometers"
67         self.beamwaist=w0
68         self.rayleigh_length=z0
69         self.beamfocus=zmin
70     return w0, z0, zmin

```

Gaussian fit

The following code (modeled after [56] allows to extract the distribution's data for any given 2D array containing a Gaussian distribution . The distribution is fitted to the function `gaussian` while the function `moments` allows estimations of the widths (σ_x , σ_y) and center (x_0 , y_0) (see Chapter 2.5). To reduce the computing speed `find_highestpeak` searches for the pixel with highest value to estimate the center position. The variable `widthguess` is an estimation by the user of the distribution's width (in pixels). The picture is then reduced by the function `imreduce` which takes the data array from the image as well as estimations for the Gaussian function - which can either be obtained by the `moments` function or `find_highestpeak`. A multiplier determines the size of the square which is cut out from the picture.

Source Code

```

1 from numpy import *
2 from scipy import optimize
3 import os
4 import numpy as np
5 from scipy.misc import imread, toimage, imshow
6 import matplotlib.pyplot as plt
7
8 def gaussian(height, center_x, center_y, width_x, width_y):
9     #Returns a gaussian function with the given parameters
10    width_x = float(width_x)
11    width_y = float(width_y)
12    return lambda x,y: height*exp(-(((center_x-x)/width_x)**2+((
        center_y-y)/width_y)**2)/2)
13
14 def find_highestpeak(data, widthguess):
15     # scans the image to find the highest peak
        intensity for image reduction
16    peak=np.amax(data)
17    index=np.where(data==peak)
18    index_x=index[0][0]
19    index_y=index[1][0]
20    params=[peak, index_x, index_y, widthguess, widthguess]
21    return params
22
23
24 def imreduce(data, params, multiplier):
25    ##To increase processing speed the previous center of the
        laser and width are used to cut out
26    ##a large part of unnecessary data (the size of this new
        array depends on the multiplier)
27    ### IMPORTANT: the multiplier has to be large enough
28    ## to cover for possible movement of the laser spot
29
30    x=params[1]
31    y=params[2]
32    w_x=params[3]
33    w_y=params[4]
34    reduced_data=data[x-abs(multiplier*w_x):x+abs(multiplier*w_x
        ), y-abs(multiplier*w_y):y+abs(multiplier*w_y)]

```



```

35
36     return reduced_data
37
38 def moments(data):
39     # returns (height, x, y, width_x, width_y)
40     total = data.sum()
41     X, Y = indices(data.shape)
42     x = (X*data).sum()/total
43     y = (Y*data).sum()/total
44     col = data[:, int(y)]
45     if col.sum()==0:
46         print "System Failure"
47         return
48     width_x = sqrt(abs((arange(col.size)-y)**2*col).sum()/col.
49                    sum()))
49     row = data[int(x), :]
50
51     if row.sum()==0:
52         print "System Failure"
53         return
54     width_y = sqrt(abs((arange(row.size)-x)**2*row).sum()/row.
55                    sum()))
55     height = data.max()
56     return height, x, y, width_x, width_y
57
58 def fitgaussian(data, params):
59     # Returns the gaussian parameters of a 2D distribution found
60     # by a fit
61     errorfunction = lambda p: ravel(gaussian(*p)(*indices(
62         data.shape)) - data)
61     p, success = optimize.leastsq(errorfunction, params)
62     return p

```

Waveplate

This code was chosen as a representative example for the measurement structure. The same structure was used for the beam profiler and pulsed Z-Scan. Using `pyqtSignal` the class is emitting signals to the GUI which in turn reacts to these signals. The signal “started” indicates that the measurement has commenced and all parameters reset. After each measurement “progress” sends the measured data to the GUI so that the plot is updated after each step. The final signal “finished”

triggers the curve fitting algorithm which is then plotted in addition to the measurements. This working principle was then adapted for the beam profiler and the pulse triggered Z-Scan. The class is also depending on a second class `powermeter` which dynamically reads the measured power from a .csv file created by the Fieldmax II powermeter.

Source Code

```

1  class WaveplateCalibration(QObject):
2      finished = pyqtSignal()
3      progress = pyqtSignal(float)
4      started=pyqtSignal(bool)
5
6      def __init__(self, rot_stage, powermeter):
7          QObject.__init__(self)
8
9          self.rot_stage=rot_stage
10         self.powermeter = powermeter
11         self.iteration=0
12         self.parameters={}
13         self.load_config()
14         self.wavelength=800
15         self.cont=True
16         self.rotation=120.0
17
18         def getWavePlateParams(self, wavelength):
19             #loads the waveplate parameters if they have been saved
20             #into the library
21             if wavelength in self.parameters.keys():
22                 WavePlateParams=self.parameters[wavelength]
23                 return WavePlateParams
24
25             else:
26                 #print "Wavelength %i mm not in APT config file ,
27                 #please calibrate for this wavelength"%wavelength
28                 return None
29
30         #-----functions communicating with GUI -----
31
32         def start_calibration(self, num_points, wavelength):
33             #preparing all parameters

```

```

32     #after preparation timer is started to begin the
        measurement
33     #emits STARTED
34     self.wavelength=wavelength
35     self.started.emit(True)
36     print "start calibration"
37
38     self.num_points=num_points
39     self.stepsize = self.rotation/num_points
40     self.iteration=0
41     print "stepsize:",self.stepsize ,"num_points=", num_points
42     self.power_measurement=[]
43     self.distance_measurement=[]
44     self.appt_timer = QTimer()
45     self.appt_timer.timeout.connect(self.measure_and_move)
46     self.appt_timer.start(5000)
47     self.cont=True
48
49     def measure_and_move(self):
50         #reads the current power from the "log.csv" file which
            is generated by the powermeter class
51         #after the data has been read the waveplate is rotated
            to the next position
52         #progress signal is emitted to GUI
53         #emits PROGRESS
54         print "measure and move"
55         temppower=self.powermeter.measure_power("D:\FieldMax2
            Log\log.csv")
56         self.power_measurement=np.append(self.power_measurement ,
            temppower)
57         self.distance_measurement=np.append(self.
            distance_measurement , self.distance)
58         self.nextValue()
59         self.rot_stage.MOT_MoveAbsoluteEx(self.rot_stage.
            SerialNum , self.distance , False)
60         if self.cont:
61             self.progress.emit(self.iteration*1.0/self.
                num_points)
62
63     def fit_measurement(self):
64         #fits the measured data and stores the results

```

```

65     #emits FINISHED
66     try:
67         xdata=self.distance_measurement
68         ydata=self.power_measurement
69         aptdata=np.vstack((xdata,ydata))
70         print aptdata
71
72         ###get initial estimation from measurement:
73         idx_max=np.argmax(ydata)
74         idx_min=np.argmin(ydata)
75         A0_start=ydata[0]
76         A_start=ydata[idx_max]
77         period=abs(xdata[idx_max]-xdata[idx_min])*2
78         print period
79         b_start=np.pi/(period)
80         phi_start=0
81
82         p0=[A0_start,A_start,b_start,phi_start]
83
84         popt, pcov = curve_fit(self.apt_power, xdata, ydata,
85                               p0)
86
87         param = fitParam(A0,A,b,phi)
88         self.parameters[self.wavelength]=popt.tolist()
89         self.save_config(self.parameters)
90         savedata=zip(xdata,ydata)
91         np.savetxt("APT_Measurements.txt",savedata)
92         #emit signals
93         self.finished.emit()
94
95     except RuntimeError:
96         print "not enough Data for the fit"
97
98     def distance(self):
99         return self.iteration*self.stepsize
100
101     def cancelCalibration(self):
102         self.apt_timer.stop()
103
104     def nextValue(self):
105         #this function progresses to the next measurement

```

```

105     #if final measurement has been done the timer is stopped
106     if self.iteration<self.num_points:
107         self.iteration+=1
108         print "next value: %i"%self.iteration
109         print "distance: ",self.distance
110         return False
111     else:
112         print "end calibration"
113         self.appt_timer.stop()
114         self.fit_measurement()
115         self.cont=False
116         return True
117
118     #——functions for APT waveplate class——
119
120     def aptRotateAbsolute(self ,move):
121         #rotate APT to absolute position
122         self.rot_stage.MOT_MoveAbsoluteEx(self.rot_stage.
            SerialNum, move, False)
123
124     def aptRotateRelative(self ,move):
125         #rotate APT relative
126         self.rot_stage.MOT_MoveRelativeEx(self.rot_stage.
            SerialNum, move, False)
127
128
129     def aptHoming(self):
130         #get homing parameter to get correct angle of APT
            rotational stage
131         self.rot_stage.MOT_GetHomeParams(self.rot_stage.
            SerialNum)
132         self.rot_stage.MOT_MoveHome(self.rot_stage.SerialNum)
133
134     #——theory for power after waveplate depending on rotation
            angle——
135
136     def apt_power(self ,theta ,A0,A,b,phi):
137         #function giving the laser power depending on the
            parameters:
138         """
139         @param theta:

```

```

140     @param A0: offset from 0 Value
141     @param A: Amplitude
142     @param b: pi/Period
143     @param phi: phaseshift
144     @return:
145     """
146     return A0+A*(np.sin(b*theta+phi)**2)
147
148     #—————functions using config library—————
149
150     def load_config(self, filename="Results\cal_waveplate.yml"):
151         #if previous data exists it is loaded into the class
152         if os.path.isfile(filename):
153             with open(filename, "r") as f:
154                 self.parameters = load(f, Loader=Loader)
155                 print "loaded Previous APT Data"
156         else:
157             print "no previous APT Data"
158
159
160     def save_config(self, data, filename="Results\cal_waveplate.
161                    yml"):
162         #saves config to file
163         with open(filename, "w") as f:
164             dump(data, f, default_flow_style=False)
165         return 0
166
167     def getFittedFunction(self, xdata, wavelength):
168         param = self.parameters[wavelength]
169         if param == None:
170             return np.zeros_like(xdata)
171         A0, A, b, phi = param
172         return self.apr_power(xdata, A0, A, b, phi)
173
174     def findLaserPowerfromAngle(self, wavelength, angle):
175         #calculates the laser power from the current angle of
176         #the rotational stage
177         #Sees if a library exists for the given wavelength
178         WavePlateParams=self.getWavePlateParams(wavelength)
179         if WavePlateParams==None:
180             return

```

```

179     #if library exists the angle is calculated from the
        stored waveplate parameters
180     power=self.appt_power(angle, WavePlateParams[0],
        WavePlateParams[1], WavePlateParams[2], WavePlateParams
        [3])
181     return power
182
183     def findAngleForLaserPower(self, wavelength, power, accuracy
        =2000):
184         #read from the APT Waveplate Config File to get
            parameters and set the waveplate to the desired power
185         WavePlateParams=self.getWavePlateParams(wavelength)
186         print "Power: ", power
187         print "Waveplateparams ", WavePlateParams
188         if WavePlateParams!=None:
189             theta=np.linspace(0,120,num=accuracy)
190             power_simulated=self.appt_power(theta,*
            WavePlateParams)
191             idx_p=self.find_nearest(power_simulated, power)
192             return theta[idx_p[0]], self.appt_power(theta[idx_p
            [0]],* self.parameters[wavelength])
193         else:
194             return None

```

Cross Section Fit

The following code is used by the main Z-Scan window (Fig. S1) to extract the cross section σ_2 from the measurements (model for transmission taken from Chapter 2.2.3).

Source Code

```

1 import matplotlib.pyplot as plot
2 import numpy as np
3 from scipy.optimize import curve_fit
4 from astropy import constants as const
5 from astropy import units as u
6
7 z0 = 2.4
8
9 def fit_func(z, q0, off, amp):

```

```

10     T = 0
11     # sum
12     for m in range(0,4):
13         T+=(-q0)**m/((1+(z-off)**2/z0**2)**m*(m+1)**1.5)
14     return np.array(T*amp)
15
16 def normalizeData(data):
17     # find offset on the edges
18     left = data[0:len(data)/10]
19     right = data[-len(data)/10:-1]
20     mean = (np.mean(left)+np.mean(right))/2
21     return data/mean
22
23 def fitData(z, data):
24     # divide data by this offset
25     # ndata = self.normalizeData(z, data)
26
27     params = curve_fit(fit_func, z, data, (0,0,0.15))
28     [q0, off, amp] = params[0] # fits Rayleigh length, offset
29     and q0
30     return (q0, off, amp)
31
32 def loadData(file):
33     z, data = np.loadtxt(file, unpack=True) # unpack separates
34     in x and y
35     return (z, data)
36
37 def getCrossection(z, data, wavelength, pulseWidth, power,
38     initiatorConcentration, M2, sampleLen, replate=80):
39
40     q0, off, amp = fitData(z, data)
41     print "-----Fitted data-----"
42     print "Rayleigh range: %f mm" %z0
43     print "Offset: %f mm" %off
44     print "q0: %f" %q0
45     print "Amplitude: %0.3f" %amp
46
47     # input
48     print "-----Inputs-----"
49     wavelength=wavelength*u.mm # nm
50     print "wavelength: %f um" %wavelength.value

```



```

48 pulseWidth=pulseWidth*u.fs
49 print "pulsewidth: %f fs" %pulseWidth.value
50 power = power*u.W
51 pulsE = power/(reprate*u.MHz)# u.nJ # 115nJ
52 print "Pulse energy %f nJ" %pulsE.to(u.nJ).value
53 initiatorConcentration = (initiatorConcentration*u.mmol)/u.l
    # mM/l
54 print initiatorConcentration
55 sampleLen = sampleLen*u.mm
56 zr = z0*u.mm
57 absorption = 0.01/u.mm
58
59
60 print "———calculation of values———"
61 radius = np.sqrt(zr*wavelength/np.pi)
62 print "beam waist radius: %s" %(radius.to(u.um))
63 effectiveLen=(1-np.exp(-absorption*sampleLen))/absorption
64 print "effective length: %f" %effectiveLen.to(u.mm).value
65 PeakPow =(0.94*pulsE/pulseWidth).to(u.MW)
66 print "Peak Power: %.4g %s" %(PeakPow.value, PeakPow.unit)
67 # intensity=9528.65 # MW/cm^2
68 # intensity=(2*PeakPow/(radius**2*np.pi)).to(u.GW/u.cm**2) #
    W/cm^2
69 intensity=(2*PeakPow/(radius**2*np.pi)).to(u.GW/u.cm**2) # W
    /cm^2
70 print "Intensity: %.4g %s" %(intensity.value, intensity.unit
    )
71 TPAcoeff = ((q0)/(intensity*effectiveLen)) # q0
72 print "TPA Coefficient: %s" %TPAcoeff.to(u.cm/u.GW)
73 DensitInit= const.N_A*initiatorConcentration # molecules/cm
    ^3
74 print "Density initiator: %s" %DensitInit.to(1/u.mm**3)
75 photE=const.h*const.c/wavelength
76 print "Photon energy: %s" %photE.to(u.eV)
77
78 gm = 10**-50 * (u.cm**4 * u.s)
79
80 CrSec=TPAcoeff*photE/(DensitInit)
81 print "cross section : %.4g %s" %(CrSec.to(gm).value, "GM")
82
83 return (CrSec.to(gm).value, zr.value, q0, off, amp)

```

```

84
85 def plotfromtheory(power):
86     print "Power used for theory:", power
87     wavelength = 800*u.nm # nm
88     pulseLength = 70*u.fs # fs
89     concentration = 10*u.mmol/u.l # mM/l
90     M2 = 1
91     sampleLen = 1*u.mm
92     z0 = 2.1*u.mm
93     absorption = 0.01/u.mm
94     pulsE = power/(80e6*u.hertz)
95     crossection = 150*10**-50*u.cm**4*u.s # GM
96
97     radius = np.sqrt(z0*wavelength/(np.pi))
98     effectiveLen = (1-np.exp(-absorption*sampleLen))/absorption
99     print "effective length: %s" %effectiveLen.to(u.mm)
100    print "beam waist radius: %s" %(radius.to(u.um))
101    # http://www.rp-photonics.com/gaussian_pulses.html
102    PeakPow = (0.94*pulsE/pulseLength).to(u.MW)
103    print "Peak Power: %.4g %s" %(PeakPow.value, PeakPow.unit)
104    # intensity=9528.65 # MW/cm^2
105    # http://www.rp-photonics.com/spotlight_2009_10_03.html
106    intensity = (2*PeakPow/(radius**2*np.pi)).to(u.GW/u.cm**2) #
        W/cm^2
107    print "Intensity: %.4g %s" %(intensity.value, intensity.unit
        )
108    DensitInit = const.NA*concentration # molecules /cm^3
109    print "Density initiator: %s" %DensitInit.to(1/u.cm**3)
110    photE = const.h*const.c/wavelength
111    print "Photon energy: %s" %photE.to(u.eV)
112    TPAcoff = crossection*DensitInit/photE
113    print "TPA coefficient: %s" %TPAcoff.to(u.cm/u.W)
114    q0 = intensity*effectiveLen*TPAcoff # q0
115    print "q0: %s"%q0.to(u.dimensionless_unscaled)
116
117    z = np.linspace(-10,10,1001)*u.mm
118    data = fit_func_with_units(z, q0, 0*u.mm, 1)
119
120    return (z, data)

```

Bibliography

- [1] Mariacristina Rumi and Joseph W. Perry. Two-photon absorption: an overview of measurements and principles. *Adv. Opt. Photon.*, 2(4):451–518, December 2010.
- [2] Kevin D. Belfield, Mykhailo V. Bondar, Sheng Yao, Ivan A. Mikhailov, Vyacheslav S. Polikanov, and Olga V. Przhonska. Femtosecond Spectroscopy of Superfluorescent Fluorenyl Benzothiadiazoles with Large Two-Photon and Excited-State Absorption. *J. Phys. Chem. C*, 118(25):13790–13800, June 2014.
- [3] V E Centonze and J G White. Multiphoton excitation provides optical sections from deeper within scattering specimens than confocal imaging. *Biophys J*, 75(4):2015–2024, October 1998.
- [4] Lingyan Shi, Adrián Rodríguez-Contreras, Yury Budansky, Yang Pu, Thien An Nguyen, and Robert R. Alfano. Deep two-photon microscopic imaging through brain tissue using the second singlet state from fluorescent agent chlorophyll α in spinach leaf. *Journal of biomedical optics*, 66009:1, 2014.
- [5] Aleksandr Ovsianikov, Vladimir Mironov, Jürgen Stampfl, and Robert Liska. Engineering 3d cell-culture matrices: multiphoton processing technologies for biological and tissue engineering applications. *Expert Review of Medical Devices*, 9(6):613–633, November 2012.
- [6] S. Maruo and J.T. Fourkas. Recent progress in multiphoton microfabrication. *Laser & Photonics Review*, 2(1-2):100–111, April 2008.
- [7] A. Ovsianikov, M. Malinauskas, S. Schlie, B. Chichkov, S. Gittard, R. Narayan, M. Löbler, K. Sternberg, K.-P. Schmitz, and A. Haverich. Three-dimensional laser micro- and nano-structuring of acrylated poly(ethylene glycol) materials and evaluation of their cytotoxicity for tissue engineering applications. *Acta Biomaterialia*, 7(3):967–974, March 2011.

- [8] Xiao-Hua Qin, Aleksandr Ovsianikov, Jürgen Stampfl, and Robert Liska. Additive manufacturing of photosensitive hydrogels for tissue engineering applications. *BioNanoMaterials*, 15(3-4), January 2014.
- [9] M. Dinu, F. Quochi, and H. Garcia. Third-order nonlinearities in silicon at telecom wavelengths. *Applied Physics Letters*, 82(18):2954–2956, May 2003.
- [10] Marek Samoc, Anna Samoc, Barry Luther-Davies, Zhenan Bao, Luping Yu, Bing Hsieh, and Ullrich Scherf. Femtosecond Z-scan and degenerate four-wave mixing measurements of real and imaginary parts of the third-order nonlinearity of soluble conjugated polymers. *Journal of the Optical Society of America B*, 15(2):817, February 1998.
- [11] Eric W. Van Stryland, J. Hagan Hagan, Olga V. Przhonska, Seth R. Marder, Scott Webster, and Lazaro A. Padilha. Nonlinear Absorption Spectroscopy of organic Dyes, December 2009.
- [12] Jing Liu and Jingsong Wei. Optical nonlinear absorption characteristics of AgInSbTe phase change thin films. *Journal of Applied Physics*, 106(8):083112, October 2009.
- [13] Mariacristina Rumi, Stephen Barlow, Jing Wang, Joseph W. Perry, and Seth R. Marder. Two-Photon Absorbing Materials and Two-Photon-Induced Chemistry. In Seth R. Marder and Kwang-Sup Lee, editors, *Photoresponsive Polymers I*, number 213 in Advances in Polymer Science, pages 1–95. Springer Berlin Heidelberg, 2008.
- [14] Maria Göppert-Mayer. Über Elementarakte mit zwei Quantensprüngen. *Annalen der Physik*, 401(3):273–294, 1931.
- [15] W. Kaiser and C. G. B. Garrett. Two-Photon Excitation in $\text{Ca F}_2 : \text{Eu}^{2+}$. *Physical Review Letters*, 7(6):229–231, September 1961.
- [16] Mihaela Balu, Lazaro A. Padilha, David J. Hagan, Eric W. Van Stryland, Sheng Yao, Kevin Belfield, Shijun Zheng, Stephen Barlow, and Seth Marder. Broadband Z-scan characterization using a high-spectral-irradiance, high-quality supercontinuum. *J. Opt. Soc. Am. B*, 25(2):159–165, February 2008.
- [17] Mangirdas Malinauskas, Maria Farsari, Algis Piskarskas, and Saulius Juodkazis. Ultrafast laser nanostructuring of photopolymers: A decade of advances. *Physics Reports*, 533(1):1–31, December 2013.
- [18] W. Denk, J.H. Strickler, and W.W. Webb. Two-photon laser scanning fluorescence microscopy. *Science*, 248(4951):73–76, 1990.

- [19] M. Sheik-Bahae, A.A. Said, T.-H. Wei, D.J. Hagan, and E.W. Van Stryland. Sensitive measurement of optical nonlinearities using a single beam. *IEEE Journal of Quantum Electronics*, 26(4):760–769, April 1990.
- [20] Eric W. Van Stryland and Mansoor Sheik-Bahae. Z-scan measurements of optical nonlinearities. *Characterization Techniques and Tabulations for Organic Nonlinear Materials*, pages 655–692, 1998.
- [21] A. Miller and D. M. Finlayson. *Laser Sources and Applications*. CRC Press, January 1997.
- [22] Aleksei Zheltikov, Anne LHuillier, and Ferenc Krausz. Nonlinear Optics. In Frank Traeger Prof, editor, *Springer Handbook of Lasers and Optics*, pages 157–248. Springer New York, 2007.
- [23] Orazio Svelto. *Principles of Lasers*. Springer Science & Business Media, March 2010.
- [24] M. Sheik-Bahae, J. Wang, R. DeSalvo, D. J. Hagan, and E. W. Van Stryland. Measurement of nondegenerate nonlinearities using a two-color Z scan. *Optics letters*, 17(4):258–260, 1992.
- [25] rp-photonics.com. Peak power. http://www.rp-photonics.com/peak_power.html. [Online; accessed 08-Mai-2015].
- [26] Max J. Riedl. *Optical design fundamentals for infrared systems*. Number TT 48 in Tutorial texts in optical engineering. SPIE Press, Bellingham, Wash, 2nd ed edition, 2001.
- [27] Thorlabs. Be04r/m - 4x reflective optical beam expander. <https://www.thorlabs.com/thorproduct.cfm?partnumber=BE04R/M>. [Online; accessed 09-Mai-2015].
- [28] rp photonics.com. Focal Length. http://www.rp-photonics.com/focal_length.html. [Online; accessed 08-May-2015].
- [29] Michael Bass and Optical Society of America, editors. *Handbook of optics*. McGraw-Hill, New York, 2nd ed edition, 1995.
- [30] Bahaa E. A. Saleh. *Fundamentals of photonics*. Wiley series in pure and applied optics. Wiley Interscience, Hoboken, N.J, 2nd ed edition, 2007.
- [31] Devraj Singh. *Fundamentals of Optics*. Prentice-Hall of India Pvt.Ltd, August 2010.

- [32] Mauro Falconieri. Thermo-optical effects in Z -scan measurements using high-repetition-rate lasers. *J. Opt. A: Pure Appl. Opt.*, 1(6):662, November 1999.
- [33] R. de Nalda, R. del Coso, J. Requejo-Isidro, J. Olivares, A. Suarez-Garcia, J. Solis, and C. N. Afonso. Limits to the determination of the nonlinear refractive index by the Z-scan method. *Journal of the Optical Society of America B*, 19(2):289, February 2002.
- [34] C. Jacinto, D. N. Messias, A. A. Andrade, S. M. Lima, M. L. Baesso, and T. Catunda. Thermal lens and Z-scan measurements: Thermal and optical properties of laser glasses – A review. *Journal of Non-Crystalline Solids*, 352(32–35):3582–3597, September 2006.
- [35] E. Marín. Characteristic dimensions for heat transfer. *Latin-American Journal of Physics Education*, 4(1):56–60, 2010.
- [36] Andrea Gnoli, Luca Razzari, and Marcofabio Righini. Z-scan measurements using high repetition rate lasers: how to manage thermal effects. *Optics Express*, 13(20):7976, 2005.
- [37] Ming-Kuei Hu. Visual pattern recognition by moment invariants. *IRE Transactions on Information Theory*, 8(2):179–187, February 1962.
- [38] José Antonio Martín H., Matilde Santos, and Javier de Lope. Orthogonal variant moments features in image analysis. *Information Sciences*, 180(6):846–860, March 2010.
- [39] D. E. Spence, P. N. Kean, and W. Sibbett. 60-fsec pulse generation from a self-mode-locked Ti:sapphire laser. *Opt. Lett.*, 16(1):42–44, January 1991.
- [40] J.D. Kafka, M.L. Watts, and J.-W.J. Pieterse. Picosecond and femtosecond pulse generation in a regeneratively mode-locked Ti:sapphire laser. *IEEE Journal of Quantum Electronics*, 28(10):2151–2162, October 1992.
- [41] Spectra Physics. MaiTai DeepSee Data Sheet. <http://www.spectra-physics.com/products/ultrafast-lasers/mai-tai-deepsee>. [Online; accessed 02-Mai-2015].
- [42] Eugene Hecht. *Optics*. Addison-Wesley, Reading, Mass, 4th ed edition, 2002.
- [43] H. Gordon Berry, G. Gabrielse, and A. E. Livingston. Measurement of the Stokes parameters of light. *Applied optics*, 16(12):3200–3205, 1977.

- [44] John M. Khosrofian and Bruce A. Garetz. Measurement of a Gaussian laser beam diameter through the direct inversion of knife-edge data. *Appl. Opt.*, 22(21):3406–3410, November 1983.
- [45] IDS Imaging. UI-1580SE. <https://de.ids-imaging.com/store/ui-1580se.html>, 2015. [Online; accessed 28-April-2015].
- [46] Eric W. Weisstein. Least Squares Fitting.
- [47] Hellma Analytics. Certificate High Precision Cells. <http://www.hellma-analytics.com/text/283/de/material-und-technische-informationen.html>. [Online; accessed 29-April-2015].
- [48] M. J. Snare, F. E. Treloar, K. P. Ghiggino, and P. J. Thistlethwaite. The photophysics of rhodamine B. *Journal of Photochemistry*, 18(4):335–346, 1982.
- [49] Cornell Universtiy. Developmental Resource for Biophysical Imaging Optoelectronics. http://www.drbio.cornell.edu/cross_sections.html. [Online; accessed 02-Mai-2015].
- [50] Naga Srinivas Narayana Rao N. K. M. D. Venugopal Rao S. Nonlinear absorption and excited state dynamics in Rhodamine B studied using Z-scan and degenerate four wave mixing techniques. *Chemical Physics Letters*, 361:439–445, 2002.
- [51] Katherine J Schafer, Joel M Hales, Mihaela Balu, Kevin D Belfield, Eric W Van Stryland, and David J Hagan. Two-photon absorption cross-sections of common photoinitiators. *Journal of Photochemistry and Photobiology A: Chemistry*, 162(2-3):497–502, March 2004.
- [52] Peter Kapusta. Absolute Diffusion Coefficients: Compilation of Reference Data for FCS Calibration. http://www.picoquant.com/images/uploads/page/files/7353/appnote_diffusioncoefficients.pdf. [Online; accessed 01-Mai-2015].
- [53] Spectra Physics. 315a Rev. A Mai Tai WB User’s Manual, 2003.
- [54] Thorlabs. APT Manual. https://www.thorlabs.de/software_pages/ViewSoftwarePage.cfm, 2015. [Online; accessed 30-April-2015].
- [55] SMAC Corporation. SMAC Controller Manual. <http://www.smac-mca.nl/Manuals.html>, 2015. [Online; accessed 30-April-2015].

- [56] SciPy.org. Cookbook/FittingData. <http://wiki.scipy.org/Cookbook/FittingData>. [Online; accessed 23-October-2014].